Technische Universiteit Delft
Faculteit der Scheikundige Technologie en der Materiaalkunde
Vakgroep Fysische en Chemische Materiaalkunde

Differential Scanning Calorimetry experiments on the glass transition of the amorphous metal $Pd_{40}Ni_{40}P_{20}$

P. Tuinstra
april 1993

afstudeerdocent: Prof. dr ir A. van den Beukel
begeleiding: dr ir J. Sietsma en ir P.A. Duine

Contents

1. Introduction

The glass transition is a typical property of an amorphous material, which is a solid material with an atomic structure that lacks periodicity. An amorphous material is made by cooling a liquid at a rate that exceeds a certain minimum (critical) cooling rate, depending on the composition of the liquid. At such a high cooling rate, the crystallization kinetics are too slow to allow crystallization to take place. The disordered atomic arrangement of the liquid is then more or less retained down to low temperature, where it is 'frozen in' *i.e.* the structure does not change anymore within a reasonable amount of time.

Well-known amorphous materials are plastics and vitrous glasses. These materials are highly resistant to crystallization, hence a relatively low cooling rate is sufficient to bring them in the amorphous state (most members of these material groups are even practically impossible to crystallize). The resistance of these materials to crystallization is caused partly by the fact that the atoms in these materials are chained together to molecules, limiting their individual mobility.

The glass transition in plastics is roughly the temperature where, during heating, the plastic loses its rigidity and becomes 'rubberlike'. The loss of the mechanical rigidity is connected to an increasing mobility of the constituent molecules of the material. Vitrous glasses exhibit a similar phenomenon, the 'weakening point', where the viscosity decreases rapidly, also due to the increasing atomic mobility.

In liquid metals, atoms in stead of (large) molecules arrange during crystallization, therefore crystallization proceeds much faster in liquid metals than with the two examples above. However, at extremely high cooling rates, some compositions of metals and metal-metalloid mixtures also become amorphous. This requires special quenching techniques, which have started to develop some 30 years ago.

Amorphous metals can also exhibit a glass transition, although in most cases crystallization prevents the completion of the glass transition.

A theoretical description of the glass transition should involve the factors that determine the atomic mobility. In the case of amorphous metals, a model called the Free Volume Theory, which involves atomic jump sites as in crystalline metals, gives a good description of the measured behaviour, and will be tested further in this study.

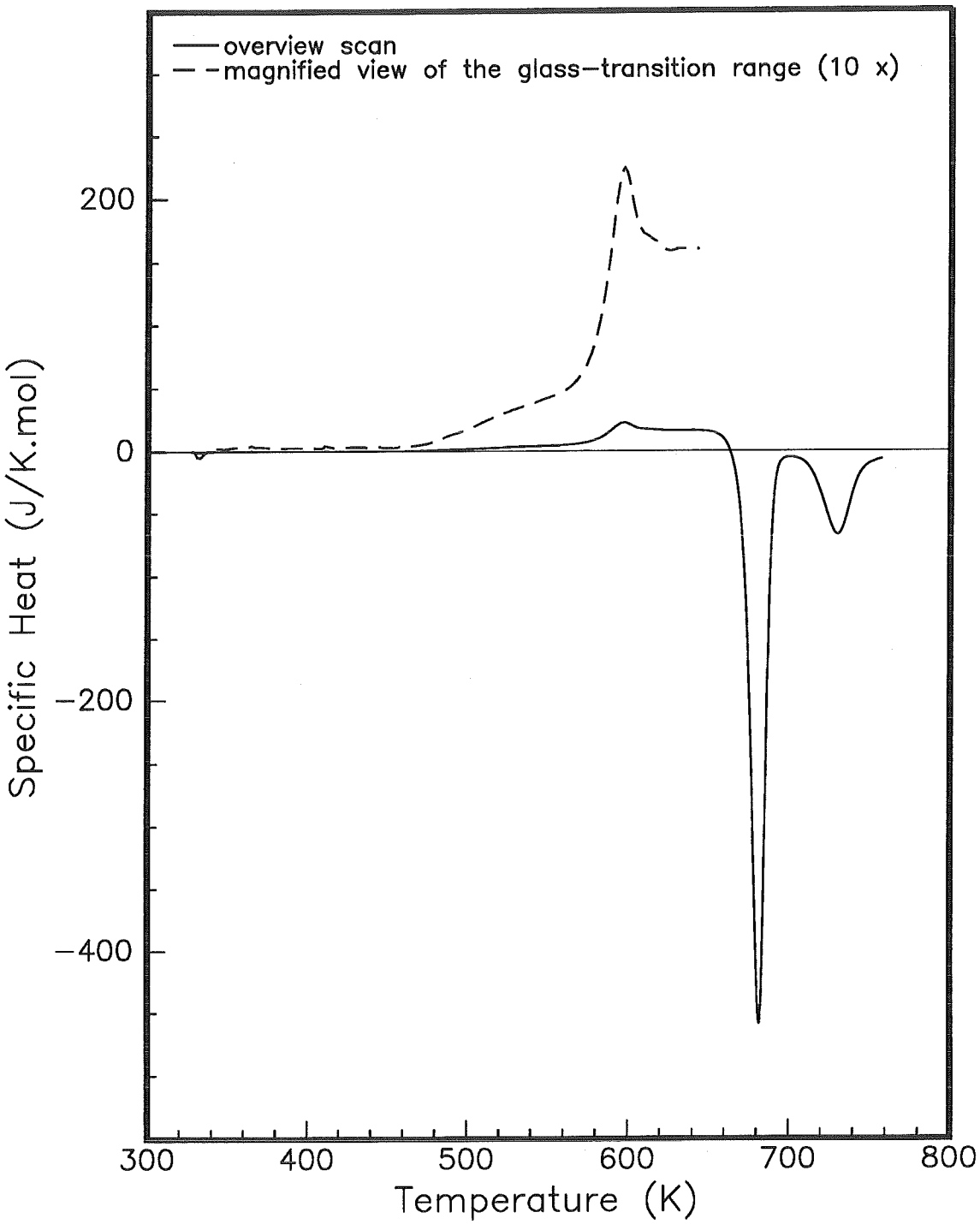

Figure 1: DSC scan of amorphous $Pd_{40}Ni_{40}P_{20}$, up to above the crystallization temperature.

The amorphous metal $Pd_{40}Ni_{40}P_{20}$, obtained by rapidly quenching a liquid that consists of 40% Pd, 40% Ni and 20% P (atomic percentages), is one of the most stable amorphous metals available. It crystallizes at a temperature well above its glass-transition range and for this reason it is well suited as a material to investigate the glass transition in amorphous metals.

In this work the thermal behaviour of $Pd_{40}Ni_{40}P_{20}$ in the glass-transition range was investigated with the Differential Scanning Calorimetry (DSC) technique. In a DSC experiment the temperature of the sample increases at a constant rate. The heat flowing to the sample is measured as a function of temperature. A graph of the heat flow versus temperature reveals a peak when a transition takes place. A graph of a complete measurement, starting at 300 K and ending at 750 K is shown in figure 1. The large peak pointing downward (exothermic) is caused by the crystallization of the material. The second exothermic peak is caused by a transition between crystalline phases.

The glass-transition peak is the small peak, pointing upwards (endothermic). The magnified view of this peak shows that after the observed transition peak, the specific heat has changed. This indicates that after the glass transition the material is in a different state than before the glass transition.

The peak itself was investigated in this work by comparing DSC measurements of material with different frozen-in states with numerical simulations based on the free volume theory.

In chapter 2 the Free Volume Theory will be discussed. It gives a description of the processes behind the observed glass transition. In chapter 3 an extensive description is given of the DSC measurement method. Finally, in chapter 4, the results of the measurements and calculations on $Pd_{40}Ni_{40}P_{20}$ are presented.

2. Theory

2.1 Introduction

Metals and metallic alloys used in practical applications have a crystalline microstructure. The crystalline microstructure has long-range translational order. In contrast to this, the arrangement of atoms in a metal above the melting temperature T_m is highly disordered.

What normally happens when a molten metal is cooled, is the formation of very small ordered regions in the liquid at a temperature just below T_m. These regions form the 'seeds' for growth of the crystalline phase. Once these 'seeds', or nucleï as they are officially called, have formed, they grow until the metal has become solid.

Because the formation of the nucleï takes time, very rapid cooling ('quenching') can prevent the formation of nucleï during cooling. When the quenching is continued to a sufficiently low temperature, the atomic mobility has become so low that the metal is apparently solid. The low atomic mobility also prevents the formation and growth of crystallites, so the metal does not crystallize any more as long as it is kept at low temperature. The material that has formed under these conditions is an amorphous metal.

The degree of disorder in the amorphous metal is variable to some extent due to the occurrence of short-range ordering (SRO). Short range ordering involves changes of the local ordering *e.g.* number and chemical species of the neighboring atoms, local bond lengths, etc., without bringing periodicity to the material as a whole.

Van den Beukel and Radelaar [1] provided a model for short-range ordering in terms of two different processes: chemical short-range ordering (CSRO) which involves changes of the chemical surrounding of the atoms, and topological short-range ordering (TSRO) which is connected to the change of the volume of the material.

As long as crystallization is prevented, the possible states of the material are the differently ordered amorphous states. At low temperature the more ordered states will be favoured, whereas at higher temperature the more disordered states will be favoured. This implies a temperature-dependent metastable equilibrium

state of the amorphous metal. The equilibrium is called metastable because the crystalline state is the true equilibrium state. According to the TSRO-CSRO model, the two ordering processes independently relax towards their equilibrium state.

The equilibrium state at room temperature is never reached in practice because the change in the order is very slow at such a low temperature. When the temperature is increased, the order starts to change towards the equilibrium value. The change of the order upon heating reveals a phenomenon called the glass transition, observable in scanning calorimetric measurements. The TSRO process dominates the thermal behaviour of the amorphous metal during the glass transition. For this reason, the experimental data on the glass transition is interpreted, using only TSRO. The next sections will deal with the theory that describes TSRO in amorphous metals, and with the glass transition as a result of changes in the TSRO state.

2.2 Free volume theory

Since the experimental data will be interpreted in terms of TSRO, only a description of TSRO will be given, following the free volume theory that was introduced by Cohen and Turnbull [3]. The influence of CSRO on the experimental DSC scan is illustrated in section 3.3 of this thesis. A detailed description of the CSRO process is given in ref. [2].

As already said, the TSRO process is connected to change of the volume of the material. The free volume theory explains changes of volume of the material with the formation and annihilation of defects in the structure. With these defects, atomic transport occurring in *e.g.* diffusion and viscosity measurements can be explained.

In a crystalline material, a defect is not difficult to indicate, it is a vacant site in the periodic lattice. In amorphous materials, it is not possible to define a defect as a vacant site in the structure, because the structure is not ordered and therefore it is impossible to observe irregularities in the structure. However, the jump mechanism is assumed to be similar to defect-governed transport in ordered structures. The definition of a jump site (defect), given in the free volume theory, is based on the volume that the atoms have at their disposal for movement.

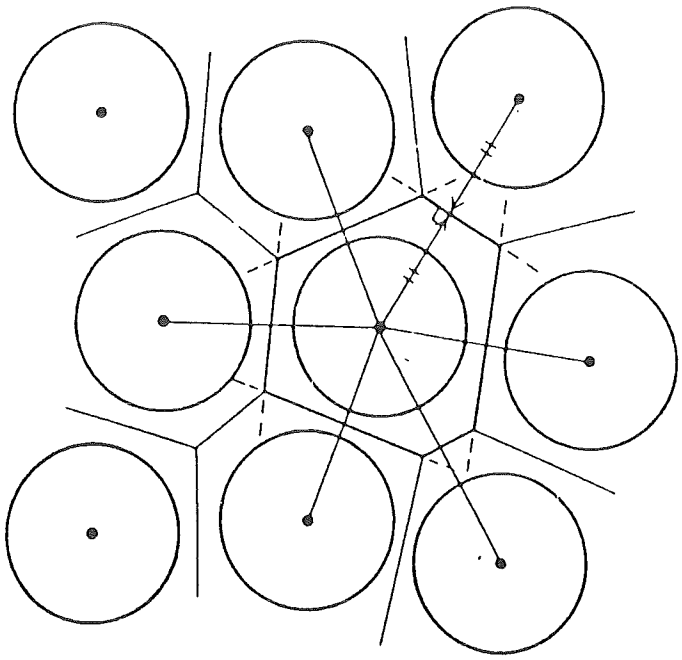

Figure 2: Principle of Wigner-Seitz cell construction (shown in two dimensions).

The volume v of an atomic site is determined by constructing a Wigner-Seitz cell around the atom, as shown in figure 2. The free volume v_f of the site in question is defined as the difference of the cell volume v and the mean cell volume v_c in a so-called ideal glass, for the structure of which no specification exists: $v_f = v - v_c$. The atomic site is considered a jump site (a defect) if the free volume v_f of the site exceeds a critical free volume, denoted by v^*. The number of jump sites per atomic site is called the defect concentration c_f. It is an important parameter, since the defects govern the ordering process.

The redistribution of the free volume v_f is assumed to take place without free energy change. With these assumptions, the distribution function $P(v_f)$ of the free volume among the atoms is given by

$$P(v_f) = \frac{\gamma}{< v_f >} \exp\left(\frac{-\gamma v_f}{< v_f >}\right), \tag{1}$$

where $< v_f >$ is the average free volume of the atoms and γ is a constant between 0.5 and 1.

The defect concentration c_f is the probability to encounter an atom with a free volume in excess of v^*:

$$c_f = \int_{v^*}^{\infty} P(v_f) dv = \exp\left(\frac{-\gamma v^*}{< v_f >}\right). \tag{2}$$

Because the variables in the argument of the exponential function cannot be separated by measurements, a quantity consisting of these variables, proportional to the average free volume $< v_f >$ is defined, which is called the reduced free volume x:

$$x = \frac{< v_f >}{\gamma v^*} = \frac{-1}{\ln(c_f)}. \tag{3}$$

In the previous section, the temperature-dependent equilibrium state of the material was already mentioned. According to the free volume theory, the equilibrium state can be associated with a temperature-dependent equilibrium defect concentration $c_{f,eq}(T)$. Experiments [4] show, in reasonable agreement with the theory, that the corresponding equilibrium value $x_{eq}(T)$ is best described by a quadratic temperature dependence, which can be approximated successfully by a linear temperature dependence for amorphous metals, because the temperature range where changes in c_f can be observed is narrow:

$$x_{eq}(T) = \frac{T - T_0}{B}, \tag{4}$$

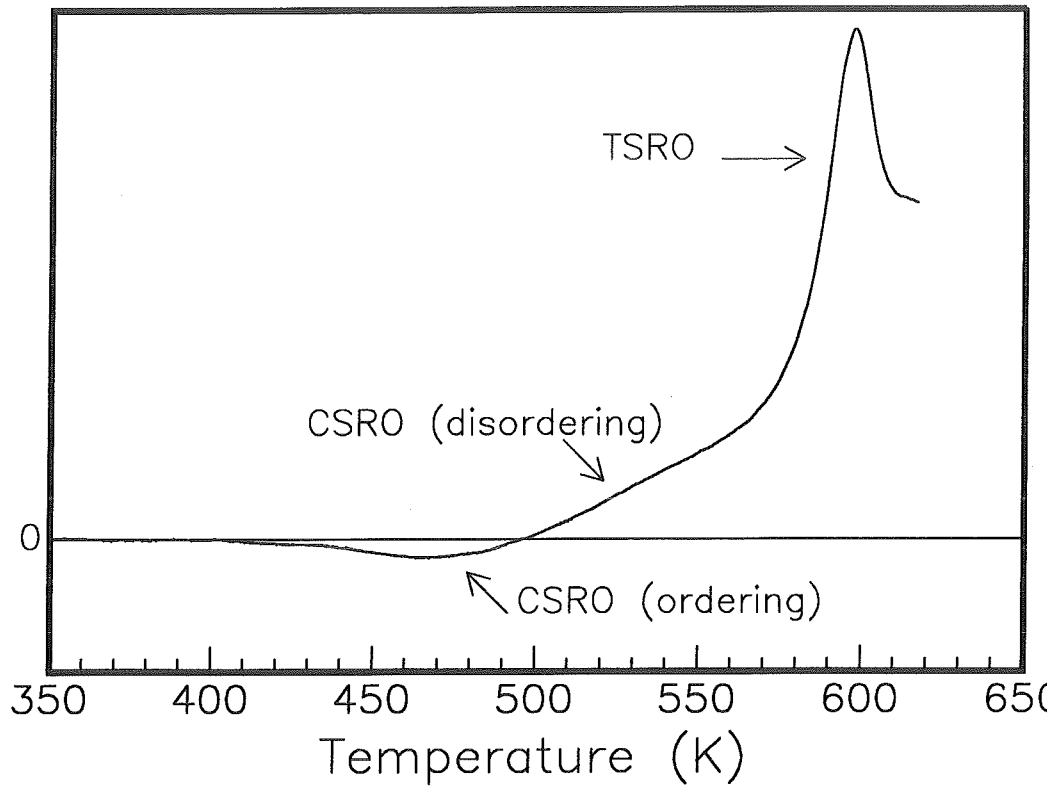

Figure 3: Measured heat-effect in an amorphous sample at constant-rate heating.

where T_0 and B are parameters which are to be determined by measurements. The rate of change of the defect concentration towards equilibrium is temperature dependent. The change towards equilibrium, called structural relaxation, is a dynamical process of annihilation and production of defects. At the equilibrium, the two competing processes have the same rate. Viscosity measurements far from the equilibrium, *e.g.* [5], show that the viscosity increases linearly with time during annealing, which implies that the annihilation rate of defects is proportional to c_f^2. Assumptions on how the production of defects takes place yield a number of different equations on the rate of change of the defect concentration. A comparison between the different equations and their ability to describe experimental results is found in [2]. The rate equation that describes the experimental results best is:

$$\frac{dc_f}{dt} = -k_f c_f (c_f - c_{f,eq}). \tag{5}$$

The factor k_f accounts for the temperature dependence of the relaxation process:

$$k_f = C_0 . \exp\left(\frac{-E_f}{RT}\right). \tag{6}$$

Here, C_0 is a constant and E_f is the activation energy for the production or the annihilation of a defect.

2.3 The glass transition

Calorimetric experiments of amorphous samples with a constant heating rate reveal an endothermic (heat-consuming) process with a maximum rate at a certain temperature. An example of such a peak is given in figure 3. In this case, the material was annealed prior to the DSC measurement, to produce an initial free volume of 0.0328. The observed endothermic peak is called the glass-transition peak. As indicated in the graph, the glass transition peak is the result of TSRO. The heat-effects preceding the actual glass transition peak are caused by CSRO. It will now be shown, that TSRO gives a good description of the glass transition. An assumption is required on how the observed heat effect is connected to the change in x. Van den Beukel and Sietsma [6] proposed the assumption that the contribution of free-volume changes to the specific heat is proportional to the rate of change of the reduced free volume. Under constant rate heating the heat flow

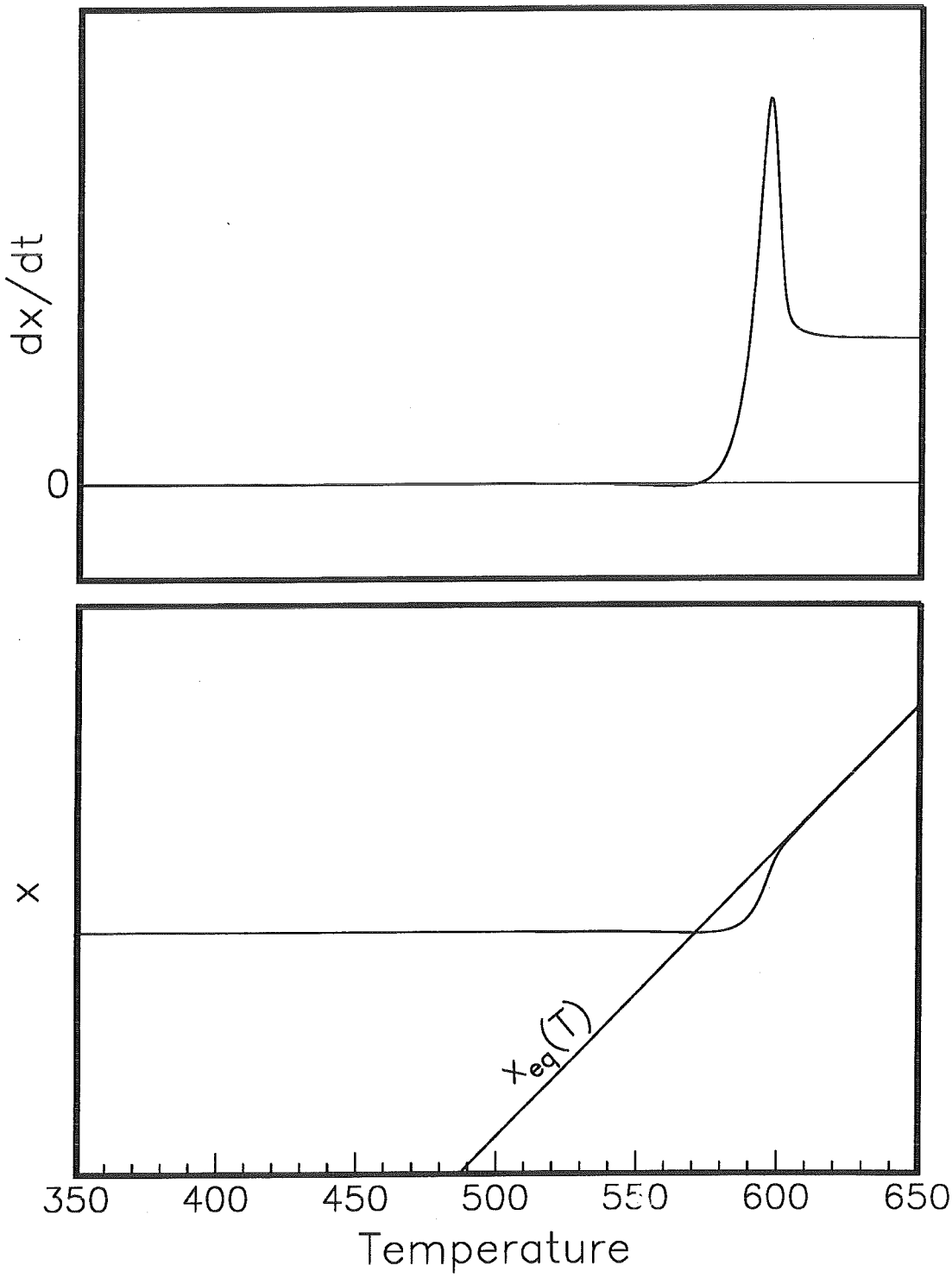

Figure 4: Example of the change of x and $\frac{dx}{dt}$ at constant-rate heating (calculation).

$\frac{dQ}{dt}$ is proportional to the specific heat, which leads to

$$\frac{dQ}{dt} \propto \frac{dx}{dt}. \tag{7}$$

The change of x in the course of the continuous-heating run is drawn with respect to the temperature-dependent value of x_{eq} in the lower part of figure 4. The changes in x follow directly from the equations (3) to (6) and the initial value of x, which was 0.0328.

At low temperature the free volume of a sample is higher than the equilibrium value for that temperature. Upon temperature increase, the relaxation rate will increase due to the strong temperature dependence of the factor k_f. The sample will approach the (changing) equilibrium value with increasing rate, thus generating increasingly more heat until x gets so close to $x_{eq}(T)$ that the heat generation diminishes. At a certain temperature the equilibrium line is reached, where the generation of heat stops. However, because of the continuously changing equilibrium, the free volume has to increase from this point on, which causes the absorption of heat. The heat absorption increases up to a maximum, which is controlled by the rate equation (5). After the maximum, heat absorption decreases to the level needed to keep up with the change of $x_{eq}(T)$. The curve of $\frac{dx}{dt}$ is shown in the upper part of figure 4. The curve has the same characteristics as the measured curve of $\frac{dQ}{dt}$ (figure 3), indicating that the free volume model can describe the glass-transition peak adequately under assumption of equation (7). The exact characteristics of the glass-transition peak (*e.g.* the peak temperature and the height of the peak) depend - apart from other physical parameters - on the value of x at the start of the heating run and on the heating rate β. In the experiments, the value of x at the start of the measurement can be set by annealing the sample prior to the measurement. For both dependencies, theoretical results were compared to experimental results. The results of these tests are presented in chapter 4.

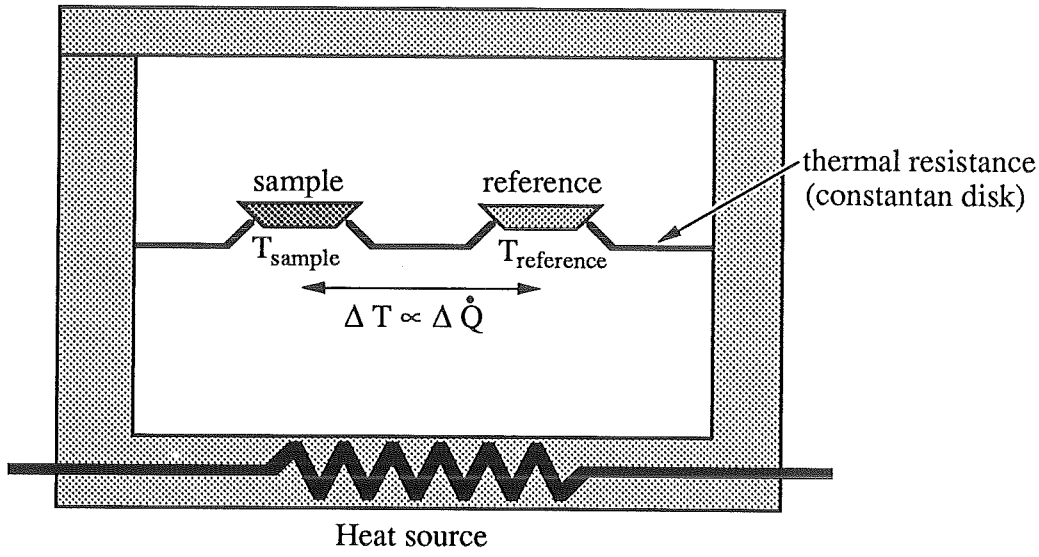

Figure 5: Schematic drawing of a heat-flux type DSC (taken from ref. [10]).

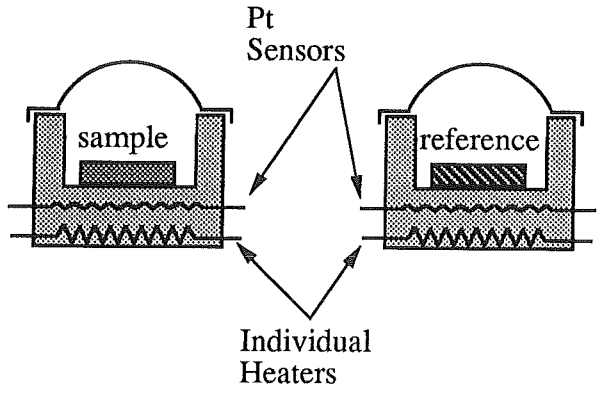

Figure 6: Schematic drawing of a power-compensated DSC (also from ref. [10]).

3. Differential Scanning Calorimetry

3.1 Introduction

The objective of Differential Scanning Calorimetry (DSC) is to measure heat effects in a sample under constant-rate heating. The heat effects are caused by transitions in the sample material, so the data obtained with the DSC technique gives information about transitions in the sample material.

The sample material is placed in a measurement device, which increases its temperature at a constant rate. The heating power supplied to the device is measured. Since the heat flow to the sample is the quantity that we are interested in, heat that is used to increase the temperature of the device itself, together with the heat loss to the surroundings of the device, must be subtracted from the total power to obtain the heat flow to the sample. The heat loss to the surroundings of the device is a complicated function of the device temperature; moreover, it can depend on parameters that change unpredictably in time, *e.g.* the ambient temperature at the moment of the measurement.

To circumvent the difficulty of determining the heat loss, the measurement is performed differentially. This means that a device called the reference device is heated simultaneously with the device containing the sample. The output signal of the DSC is the difference between the measured heating power in the sample device and the measured heating power in the reference device.

In the original instrument, called the heat-flux DSC, the heating power is determined by measuring the temperature difference over a thermal resistance. Measuring the differential heating power is then reduced to measuring the temperature difference between the sample and the reference. A drawing of the principle of a heat-flux DSC is given in figure 5.

A more recently developed type is the power-compensated type, shown schematically in figure 6. In this type, the heating power is measured by measuring the electrical power supplied to the heating coil in the device.

A drawback of the heat-flux type is that because of the way the heat flow is measured, the heating rate is truly constant only when the specific heat of the sample does not change, so when nothing happens. The variation of the heating rate is caused by lag of the sample temperature with respect to the temperature of the

heater coil. This undesirable property is called thermal lag, it causes endothermic transition peaks to become wider on the temperature scale than they would have been at constant-rate heating and exothermic peaks to become sharper.
In the power-compensated type, the lag of the sample temperature with respect to the heater temperature is smaller, causing less variation of the heating rate, as compared to the heat-flux type. A problem that rises with the power-compensated type is that due to the small thermal resistance in the device itself, the thermal resistance between the device and the sample becomes an important factor. The thermal resistance between the device and the sample depends on the shape of the sample and the way it is placed in the device, and differs between measurements. When the shape of the sample or the container changes during a measurement, *e.g.* by relaxation of internal stresses, the thermal resistance may even vary within that single measurement, causing unpredictable results for the measured heat flow. It is therefore that the measurements in a power-compensated DSC can have a poor reproducibility. Also, the electronic control circuits interact with the thermal lag of the remaining part of the instrument in a complex way. This is why the behaviour of a power-compensated DSC is much more complicated to fit into a model.
Another problem concerning the power-compensated DSC is the determination of the actual temperature of the sample. This is done in a more indirect way than with the heat-flux DSC. Because heat flows through the thermometer, there is a temperature difference between the thermometer and the sample, which depends on the selected heating rate and the heat effects in the sample.
Because it is of particular importance to know the actual sample temperature when DSC-scans of amorphous metals are used to verify the validity of the theory presented in chapter 2, an analysis of the factors that affect the temperature determination is incorporated in this chapter. In section 3.2 the working principle of the used instrument will be explained, in section 3.3 the necessary calibration of the instrument will be introduced, together with additional correction procedures, taking the thermal lag of the sample into account. Finally, in section 3.4, the free volume theory from chapter 2 will be combined with thermal lag to compare the experimental scans with their theoretical (simulated) counterparts.

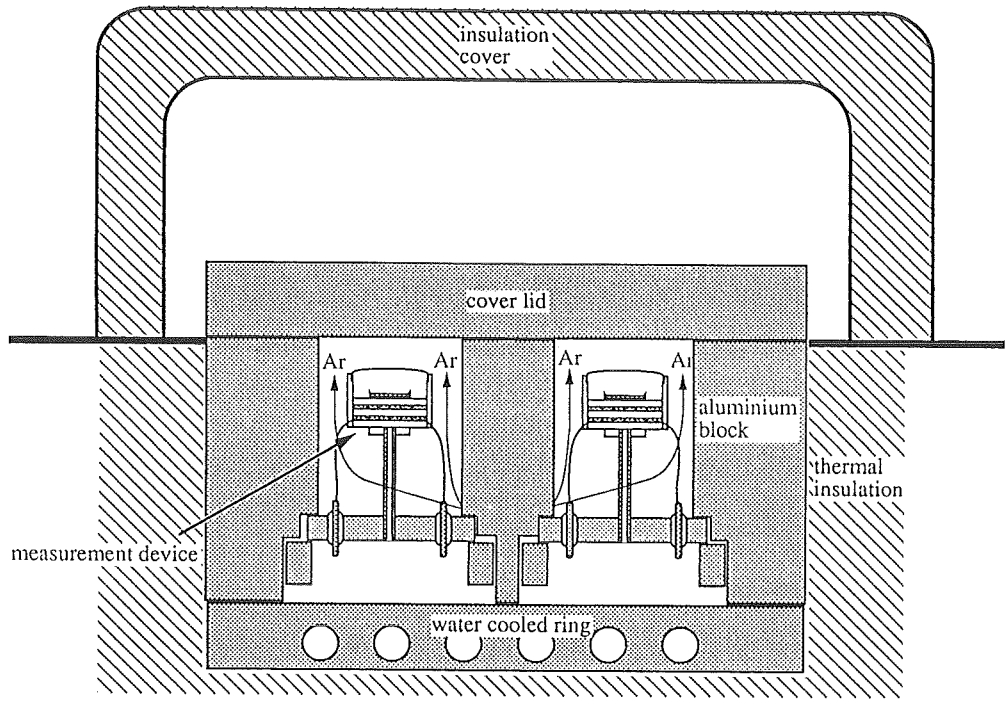

Figure 7: The two measurement devices of the DSC, positioned inside the holder.

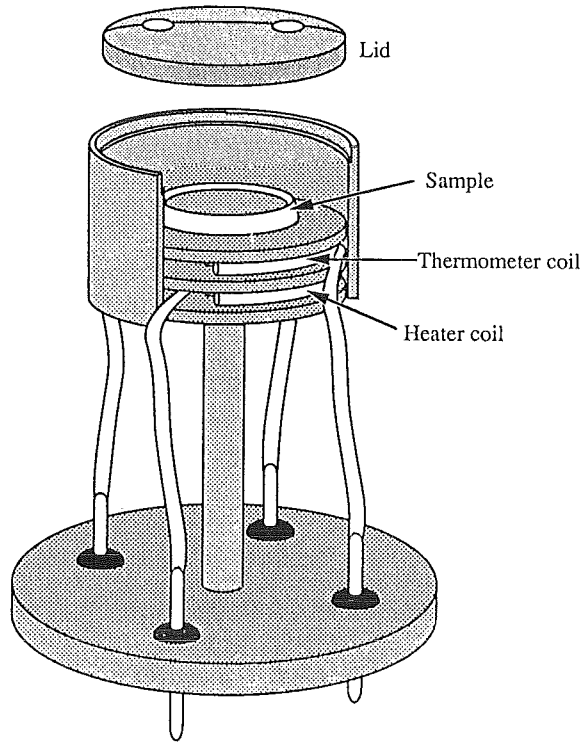

Figure 8: Separate measurement device, showing the heater coil and the platinum resistance coil of the thermometer.

3.2 Working principle of the Perkin-Elmer DSC-7

For the experiments presented in this work, we used a Perkin-Elmer DSC-7 power-compensated type DSC.

The heart of the Perkin-Elmer DSC-7 is shown in figure 7. It consists of the two measurement devices, enclosed in a holder. The devices are accessible from the outside by means of a lid that can be removed to change samples. The holder block is kept at a constant temperature (in our case just above room temperature) by means of a water-cooled ring attached to the bottom of the holder block (the temperature of the water flowing through the ring is regulated by a control unit outside the DSC instrument).

The holder block is thermally insulated from the ambient temperature by an insulating cover, positioned on top of the instrument during the scan.

To obtain a protective atmosphere inside the block, oxygen and other contaminants from the air are purged out of the system by a constant flow of purified argon gas, entering from under the measurement device and exiting through the cover lid.

A picture of a separate measurement device is given in figure 8. The construction of the device is relatively simple. It consists of two electrically insulated coils, kept together by platinum plates. The upper coil is the probe of the resistance thermometer, the lower coil is the heater coil. The temperature of the device is determined by measuring the resistance of the platinum wire. A control device supplies electrical current to the heater coil, the magnitude of which is connected to the measured temperature.

The functional units that control the power supply to the heater coils of the devices is shown schematically in figure 9.

In the centre is a program unit that controls the whole process by determining the program temperature T_p, using a clock signal and the heating rate β set by the user. It also uses the clock signal to activate alternately the two independent control units that regulate the power supply to the heater coils. First, the average temperature control unit supplies equal amounts of electric energy E_a to both heater coils to increase the average temperature of both devices to the current program temperature T_p.

After this has been done, there is a possible temperature difference between the two devices. To compensate this temperature difference, the differential control

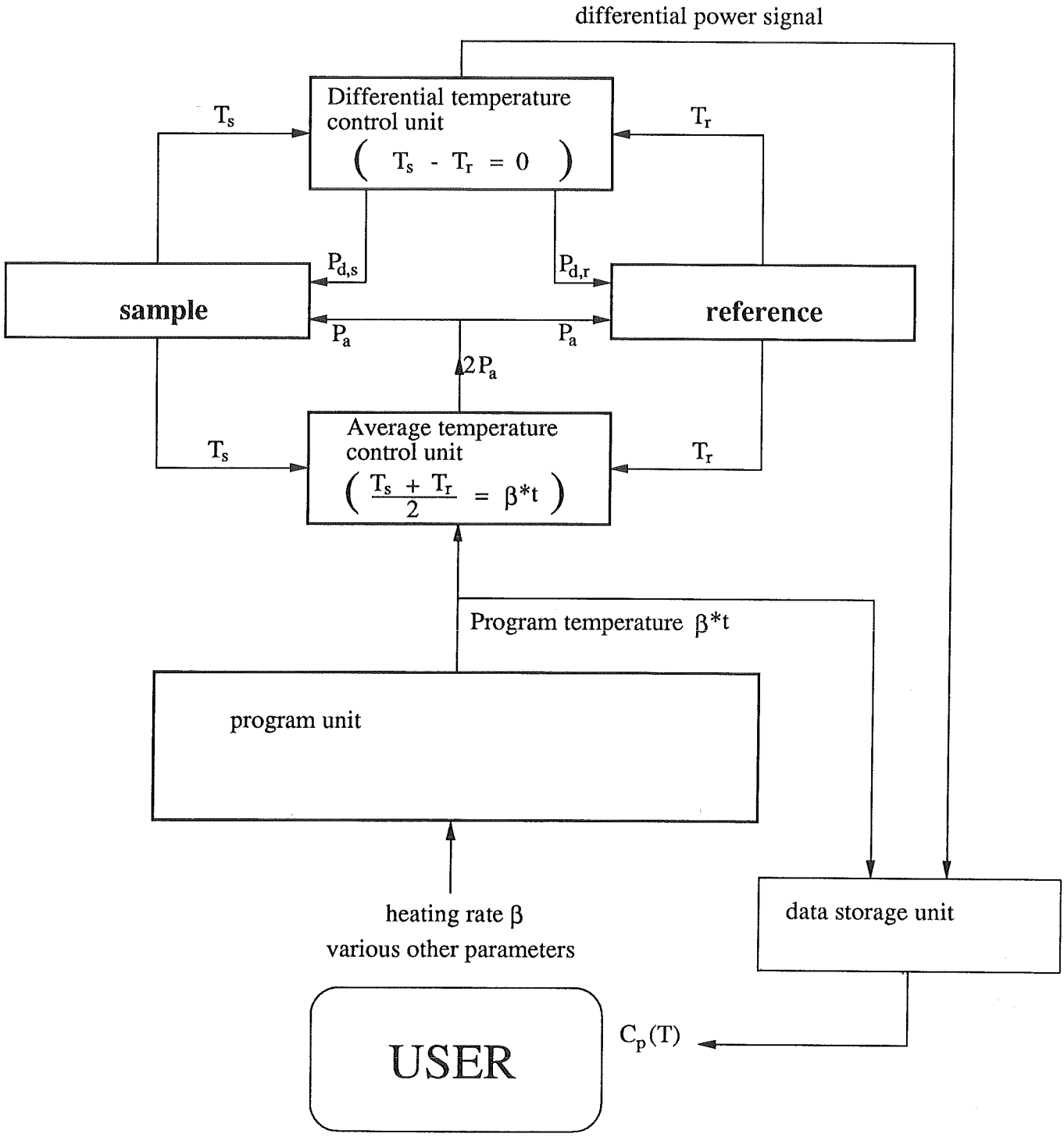

Figure 9: Diagram of the functional units in a power-compensated DSC.

unit is activated. It supplies additional amounts of electric energy $E_{d,s}$ and $E_{d,r}$ to the sample and reference heater coils, respectively.
The difference between $E_{d,s}$ and $E_{d,r}$, divided by the time that has elapsed since the average control unit was activated, is the differential power level ΔP, which is sent to the data storage unit, together with the current program temperature T_p.
It is important to realize that it is not the actual sample temperature that is recorded by the data storage unit but the program temperature, indicating that the manufacturer silently assumes the sample temperature to be equal to the program temperature under all circumstances.
Usually, the thermal lag is not taken into account, in which case the relation between the differential power $\Delta P(T)$ and the specific heat of the sample $C_{p,s}(T)$ is simple:

$$\Delta P(T) = (C_{p,s}(T)m_s - C_{p,r}(T)m_r) \cdot \beta \tag{8}$$

Or, in the case that the reference device is empty:

$$\Delta P(T) = C_{p,s}(T)m_s \cdot \beta \tag{9}$$

where m is the mass, β is the heating rate and T and t are the temperature and the time, respectively. With the value of $m_s\beta$, the measured graph of $\Delta P(T)$ is converted directly to a graph of $C_{p,s}(T)$. However, as already has been indicated, the measured value of $\Delta P(T)$ is not exactly proportional to the specific heat of the sample, due to thermal lag. This problem will be dealt with in section 3.3.2.

3.3 DSC calibration and correction procedures

3.3.1 Standard calibration and correction procedure

3.3.1.1 Calibration of a power-compensated DSC.

Because the properties of the electronic circuits that determine ΔP are not guaranteed to remain completely the same over a longer period of time, the manufacturer has chosen to enable the user to calibrate the measured value of ΔP. This calibration involves setting a calibration constant so that the recorded differential power equals the actual difference in electrical power, supplied to the devices.
The calibration can be performed in two ways: by determining the transition

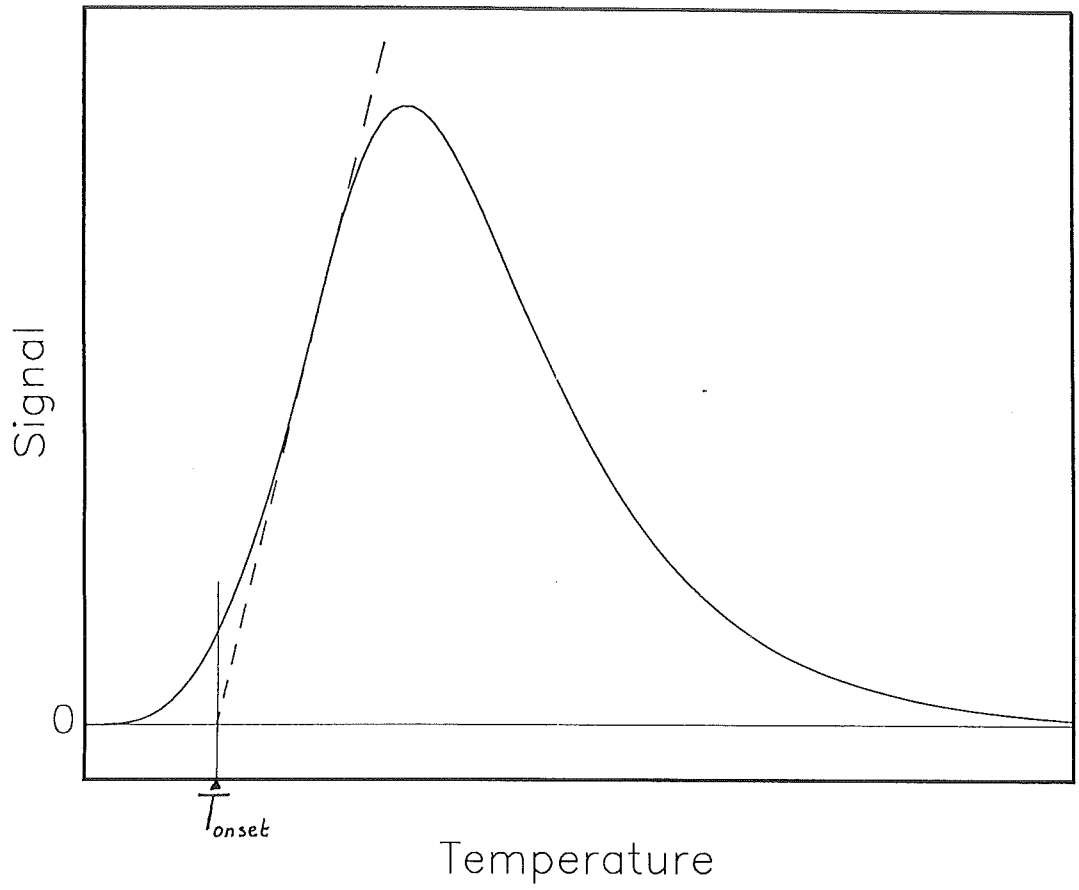

Figure 10: Practical determination of the onset temperature of a peak

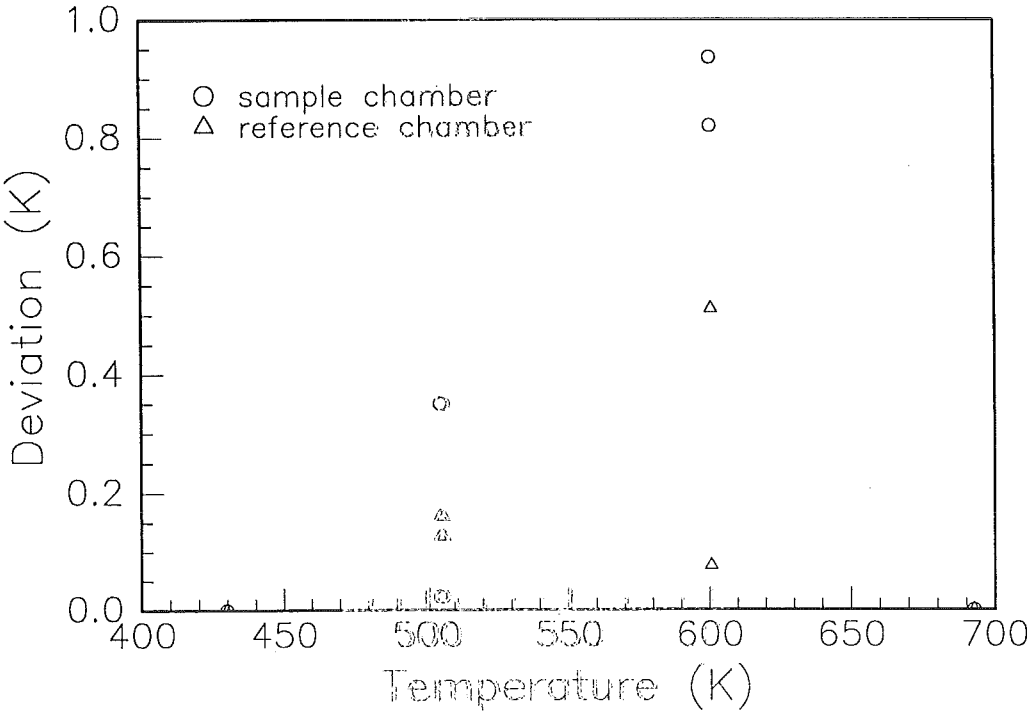

Figure 11: Difference between measured melting temperature and the literature value of the melting temperature, to determine the non-linearity of the temperature axis (see text).

heat of melting of a pure metal, or by measuring a standard material with a well-documented specific heat as a function of temperature. In the case of calibration with a pure metal, the area of the transition peak in the $\Delta P - T$ graph is determined. This should match the solid-liquid transition heat of the metal, which can be determined with other, more absolute calorimetric methods. In the case of the calibration with the standard material, the graph of $\Delta P - T$ is converted to a $C_p - T$ graph as described in section 3.2, and compared with the documented values of $C_p(T)$. It has been reported [7] that the two calibration methods can result in slightly different ($\approx 2\%$) calibration constants, most likely caused by the fact that in the transition heat calibration the heat flow to the sample during the transition is orders of magnitude higher than in the case of the calibration with the material with a known specific heat. It is therefore recommended to use the specific heat calibration when measuring the specific heat and to use the transition heat calibration when measuring the transitions heat of a material.
For this reason, we chose the transition-heat calibration method. We chose pure lead as the transition heat standard because its melting temperature lies in the glass transition range of amorphous $Pd_{40}Ni_{40}P_{20}$ (≈ 600 K).
For the temperature measurement, the need for user calibration is even more obvious. Two factors are important here: one factor is a slow change of the properties of the circuits measuring the resistance of the Pt-coil, the other factor is that the temperature difference between the thermometer and the sample varies with varying heating rate. Therefore, calibration of the temperature axis is required every time another heating rate is selected. The temperature axis is calibrated by fixing two points of the temperature axis. These points are fixed by running scans of two different pure metals to a temperature above their melting temperature T_m. The first deviation of the differential power line with respect to the extrapolated straight differential power line before melting is where the sample temperature has reached T_m. This point is the onset temperature of the melting peak, which is usually approximated by drawing the tangent at the point of inflection of the low-temperature part of the peak (see figure 10).
The linearity of the temperature axis of our instrument was checked by comparing literature values of the melting points of four different pure metals (indium, tin, lead and zinc) with experimentally determined onset temperatures of melting. This test was performed two times for both the sample device and the reference device. The result is shown in figure 11. Two points of the temperature axis can

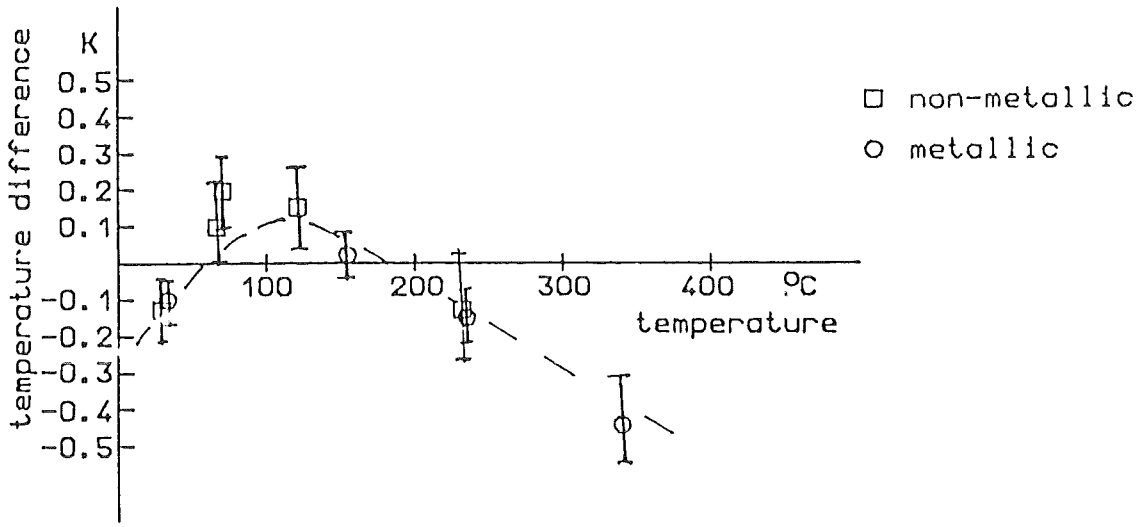

Figure 12: Same plot as figure 11, results from ref. [7].

be scaled by the user. For this test, we chose to scale the temperature axis in such a way that the experimental melting temperatures of the metals with lowest and highest melting point (indium and zinc, respectively) matched their reported literature values. These points being set (they have a value of zero in the plot), the difference between the experimentally determined melting temperatures and their literature values of the other metals can give an indication of the error in the linearity of the temperature determination.
The scans were taken at a rate of 40 K/min. It can be observed that the scatter of the data is large, in the order of magnitude of the error itself. A lower heating rate would have reduced the scatter, giving a better view of the error in the linearity of the temperature determination. Höhne and Glöggler [7] claim to find a deviation from linearity of about $\pm$ 0.2 K, using a heating rate of 10 K/min in the range between 350 and 600 K. The data they present (figure 12) indicates a non-linearity of the temperature determination in the same order of magnitude as we found ($\approx$1 K).

3.3.1.2 Baseline correction procedure

The baseline of a differential scanning calorimeter is the graph of the differential power ΔP as a function of the program temperature T_p obtained from a scan with an empty calorimeter.
Ideally, the sample and the reference device are completely identical. In that case, a scan with no material present in the devices requires the same heat flux in both devices and thus the resulting baseline of the instrument is a straight, horizontal line through the origin.
In reality the devices are not exactly similar, leading to an oblique or even a curved baseline. This undesirable effect is counteracted by electronically adding a slope and a curvature to the baseline of the instrument so that an empty scan yields a straight, horizontal $\Delta P - T_p$ line in the temperature range of interest. A drawback of this procedure is that the compensation for baseline curvature works well for the selected heating rate only. This means that every time another heating rate is selected, the baseline correction procedure must be repeated. This is one of the reasons why we chose to use a measuring method in which the baseline has minor effects on the eventual result.
Because these baseline effects are caused by differences in heat loss to the sur-

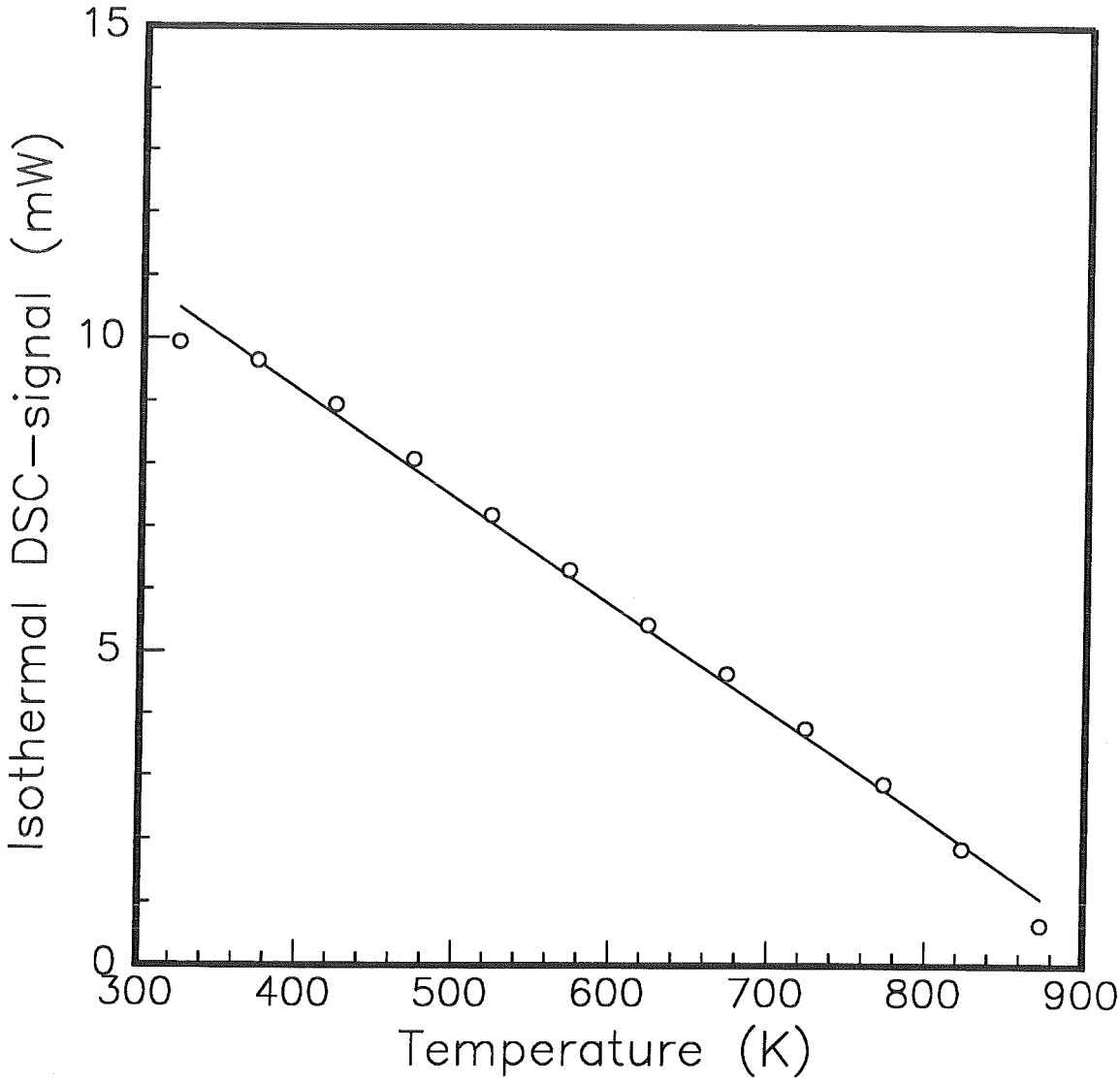

Figure 13: Isothermal differential power as a function of the temperature

roundings, it is interesting to see what the difference in heat loss is as a function of temperature. At heating rate zero (isothermal) the power flow to the device equals the heat loss to its surroundings. So the difference in heat loss to the surroundings between both devices can be measured as a function of temperature by reading the differential power at zero heating rate, at that particular temperature. This requires stabilizing at that temperature for some time, due to the thermal lag effects when heating up to that temperature.
This test was performed in the temperature range of 350 K-900 K, as shown in figure 13. The difference in heat loss is a linear function of temperature, up to about 800 K, where it starts to deviate. The linear temperature dependence of the differential power is an indication that conduction might be the dominant heat-transfer process in the observed temperature range.

3.3.2 Extended correction procedures, taking thermal lag into account

A lot of work has already been done on the determination of the quantitative reliability of DSC measurements [8], [9], [10].
The major problem in the quantitative interpretation of DSC measurements is thermal lag.
For reasons of convenience, the lag of the actual sample temperature T_s with respect to the program temperature T_p will be called thermal lag. This lag is caused by the thermal resistances together with heat capacities inside the measurement device. In addition to this, lags in the electronic control circuits may also cause thermal lag [9].
To keep the description mathematically manageable, the behaviour of the whole DSC-system, including the behaviour of the electronic circuits, was evaluated in terms of a simple R-C model. A more detailed model of the factors that affect the scans is given by Flynn (ref. [8] and ref. [9]). Applying this model to a particular instrument requires special equipment to determine a number of parameters. It is therefore that we settle here for a less refined (and less complicated) model. The proposed R-C model is an attempt to model the behaviour of the complete DSC system, hence no actual part of the DSC corresponds to the resistance or the capacity.
The temperature difference over the effective heat resistance R that connects the sample with the programmed temperature is determined by the heat flow j to

the sample:

$$T_p - T_s = R \cdot j \tag{10}$$

The heat flow into the effective capacity C of the system depends on the imposed temperature increase rate of the sample:

$$j = C \cdot \frac{dT_s}{dt} \tag{11}$$

In the course of time, the thermal lag $T_p - T_s$ increases asymptotically to its steady-state value ΔT_{st}. In the steady-state situation, the temperature increase of the sample equals the programmed heating rate β:

$$\frac{dT_s}{dt} = \frac{dT_p}{dt} = \beta. \tag{12}$$

The steady-state thermal lag of the sample ΔT_{st} can be expressed as a function of R and C and the heating rate β:

$$\frac{\Delta T_{st}}{R} = j = C \cdot \frac{dT_s}{dt} = C \cdot \beta. \tag{13}$$

The product of the resistance and the capacity RC is a time constant which will be called the retardation time τ of the system. The value of τ is a measure for the response time of the system.
Expressing the thermal lag in terms of the heating rate β and the retardation time τ of the system yields:

$$\Delta T_{st} = \beta \cdot R \cdot C = \beta \cdot \tau. \tag{14}$$

The value of ΔT_{st} can not be measured directly, but with a substance of known melting temperature, one can obtain τ and ΔT_{st} by varying β. This is done by determining the program temperature T_p^* when the sample reaches the melting temperature T_m. It is assumed that the steady-state condition has been reached before the metal starts to melt. Then the recorded temperature is the sum of the actual sample temperature and the steady-state temperature lag: $T_p^* = T_m + \Delta T_{st}$. Because T_m is known, τ can now be determined. The separate values of R and C can be obtained by increasing C with a known amount by adding material with a known specific heat to the sample. In the next section the measurements are presented that yield R and C.

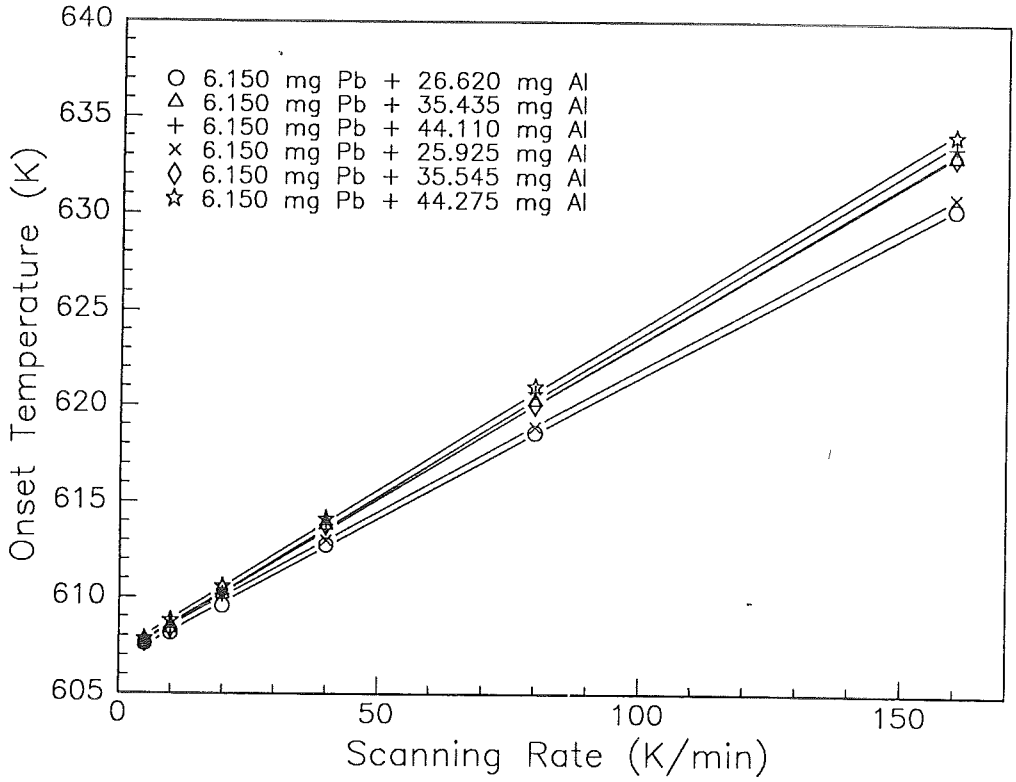

Figure 14: Measured onset temperature of the transition peak of pure lead, as a function of the heating rate, for three different values of the specific heat before melting.

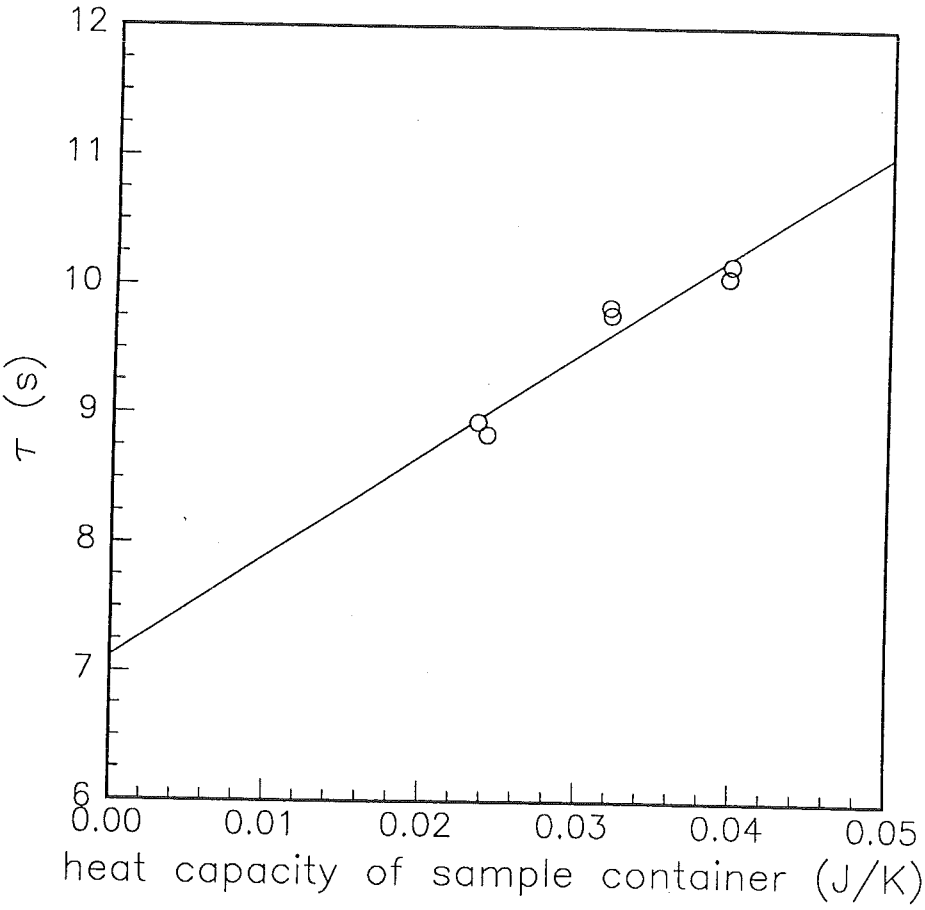

Figure 15: Retardation time τ as a function of the heat-capacity of the sample container.

3.3.3 Determination of the thermal lag in the Perkin-Elmer DSC-7

We used pure lead as the melting substance because the melting point of lead is in the glass-transition range of amorphous $Pd_{40}Ni_{40}P_{20}$.
A sample of 6.150 mg lead was put in a sample container. The recorded melting temperature T_p^* was determined at six different heating rates, from 5 K/min up to 160 K/min. This measurement was duplicated by taking the sample out of the sample chamber, putting it back in and running the six subsequent scans again. The value of C was altered by adding aluminium lids to the sample container. Each lid adds about 9 mg of aluminium, increasing the heat capacity with about 0.008 J/K. Measurements as described above were performed with one and two lids added. This results in three different values of τ due to different values of C. These measurements are shown in figure 14, where T_p^* is plotted as a function of β. If equation 14 is valid, T_p^* should be a linear function of β. This is indeed observed to be the case for this range of heating rates. The slope of the measurements with one lid on top of the sample container (the normal situation) yields $\tau = 8.75$ s.
The value of R is found by plotting the slope (which is the obtained value of τ) of the lines in figure 14 as a function of C. Because the actual value of C is not known, R is determined by plotting τ as a function of C^*, the heat capacity of the aluminium sample container (including lids), in figure 15. The predicted linearity between τ and C^* is not obvious from the plot, which is most likely caused by variation of R between measurements. The derived value of R is therefore somewhat uncertain. A value of 80 K/W matches the measured data reasonably, although any value between 50 K/W and 125 K/W is possible.
As the value of R varies between 50 K/W and 125 K/W, the corresponding value of C varies between 0.175 J/K and 0.070 J/K. Fortunately, the simulations in which these values of R and C are used, are not very sensitive to variation of R and C, as long as τ is kept constant. For the purpose of the simulations which are introduced in section 3.4, the best values for R and C, according to the data in figure 15, are used: $R = 80$ K/W and $C = 0.109$ J/K.

3.3.4 Required stabilization time of the DSC

A problem with this type of DSC is that due to the 'artificial' compensation

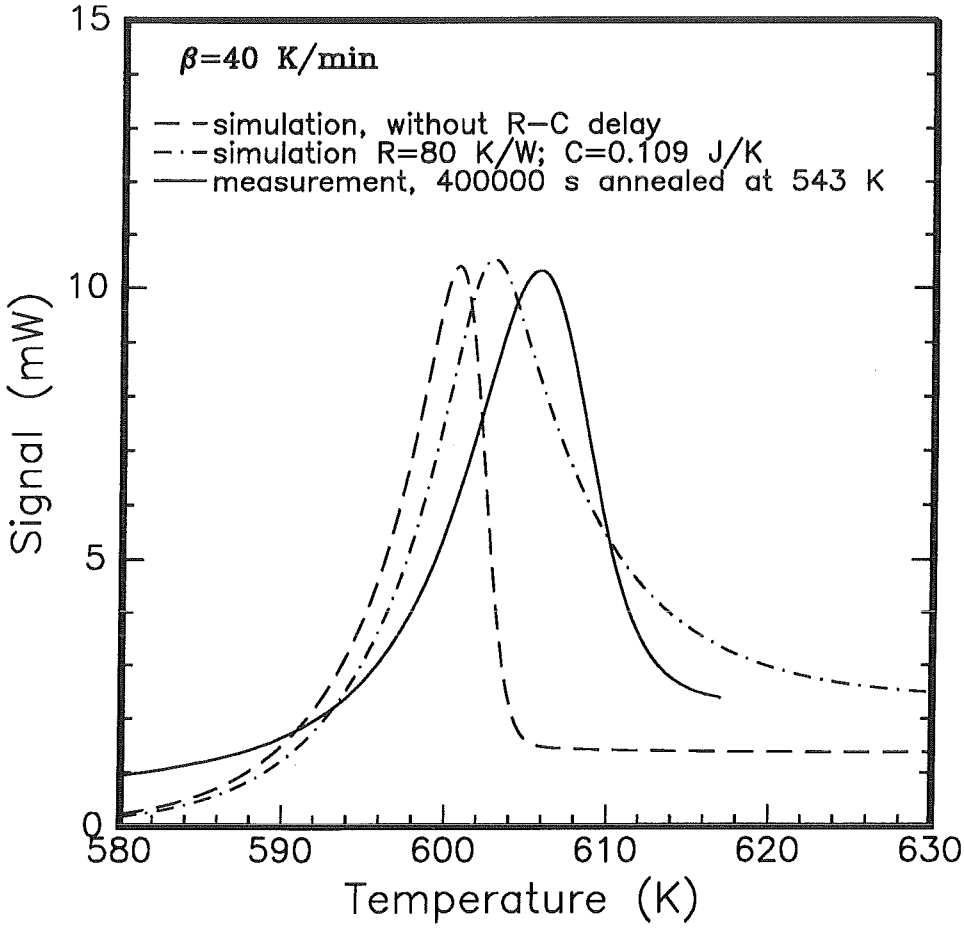

Figure 16: Experimental DSC scan of $Pd_{40}Ni_{40}P_{20}$, compared with the $C_p(T)$ graph calculated with the free volume theory, with and without taking thermal lag into account.

of the baseline, the differential power output depends on the temperature of the aluminium block. In the ideal case, the differential power should not depend on the temperature of the block because the effect should cancel out because of the differential measurement principle. Due to the electronic baseline compensation, the differential power is a function of the block temperature.
The effects of the dependence of the differential power level on the block temperature can be minimized by ensuring that the block has a homogeneous and reproducible temperature at the beginning of each scan. This can be achieved by waiting about a half an hour before starting the scan. The temperature of the block has then stabilized, providing a reproducible initial condition for the measurement.

3.4 Combining the free volume theory and the thermal lag model to predict DSC scans of amorphous metals

In order to be able to compare the experimental scans of amorphous metals with simulations of the DSC signal, the thermal lag of the DSC must be taken into account. The necessity of taking the thermal lag into account is illustrated by figure 16, where an experimental scan is compared to a calculated scan without thermal lag. The width of the calculated peak is distinctly smaller than the width of the measured peak. The calculated scan with thermal lag has a width comparable to that of the measured scan. Evidently, the broadening by thermal lag is of the same magnitude as the physical width of the glass-transition peak, indicating that thermal lag must certainly be taken into account.
With the obtained values of R and C, the heat flow j to the sample can be calculated, when the specific heat changes of the sample are known.
This has been done for the material under investigation in this work, the amorphous metal $Pd_{40}Ni_{40}P_{20}$. The specific heat of the sample is separated into two parts in this case: the part that is related to free volume changes and the part that is not related to free volume changes. The part that is not related to free volume changes is approximately 3R per mole, where R is the universal gas constant. This approximation is known as the law of Dulong and Petit and it is valid at temperatures well above the so-called Debye temperature of the material in question. Assuming that this is the case near the glass transition, in a sample of 15 mg $Pd_{40}Ni_{40}P_{20}$, the contribution is 0.005 J/K, small compared to the

0.109 J/K of the rest, it was not taken into account. The part that is related to structural relaxation is represented by a source signal $\dot{q}$, which has the same dimension as j.

As shown in equation 7, the source signal $\dot{q}$ is assumed to be proportional to the rate of change of the free volume x, which can be calculated with the rate equation (5):

$$\dot{q} = \alpha \frac{m}{M} \frac{dx}{dt}, \tag{15}$$

where α is a proportionality constant, m is the sample mass and M is the molar weight of the sample material.

A scan is simulated by assuming $T_s = T_p$ at the (low) starting temperature. A time step Δt is chosen, and T_p is increased by $\beta \Delta t$. This causes a heat flow j

$$j = \frac{T_p - T_s}{R}. \tag{16}$$

The sample temperature increases in this time step by an amount

$$\Delta T_s = \frac{j + \dot{q}}{C} \Delta t, \tag{17}$$

where $\dot{q}$ is determined by equation (15), and can be either positive or negative. This process is repeated until the final temperature for T_p is reached. The calculated heat flow j is the simulated DSC signal.

The shape of the resulting curve of j as a function of T_p depends on the proportionality constant α. A possible way to determine the value of α is to compare a simulated scan with an experimental scan. The part of the scan where the equilibrium is reached, is particularly useful for this purpose since that part does not depend on x at the beginning of the scan. In experimental scans, the specific heat in that part of the scan is about 18.3 J/(mol.K). The factor α must be adjusted in such a way that the simulated scans show the same specific heat in that part of the scan. The calculated specific heat on the equilibrium line, using equation (4), is:

$$C_{p,eq}(T) = \alpha \frac{dx_{eq}}{dT} = \frac{\alpha}{B} \Longrightarrow \alpha = C_{p,eq}(T) B. \tag{18}$$

Substitution of the value of B=6600 K in equation (18), determined by Duine [11] et al., yields α=121 kJ/mol.

This is substantially higher than the value reported by Van den Beukel and Sietsma [6], who found about 40 kJ/mol. Most of the difference however, can be explained by the fact that another value of the constant B was used.

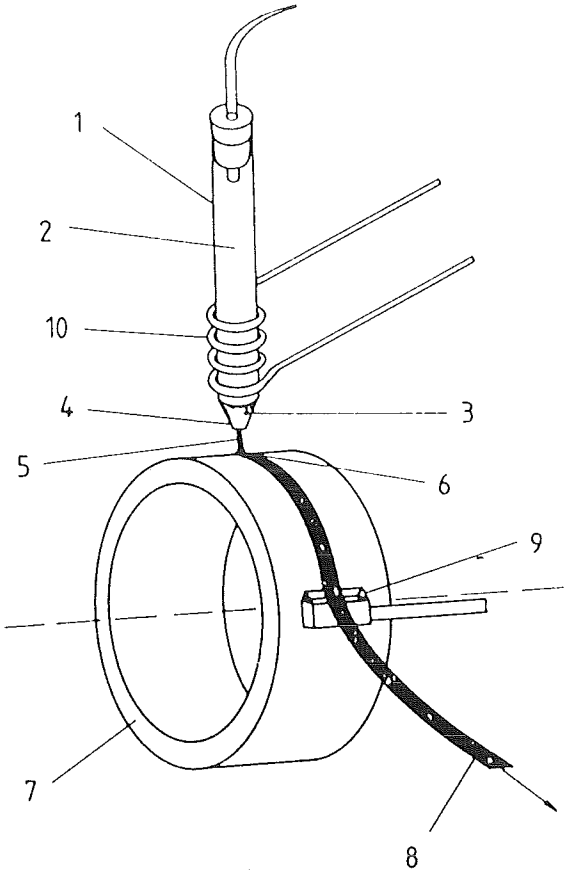

5 - liquid material; 7 - wheel; 8 - ribbon;

Figure 17: Principle of the melt-spinning method.

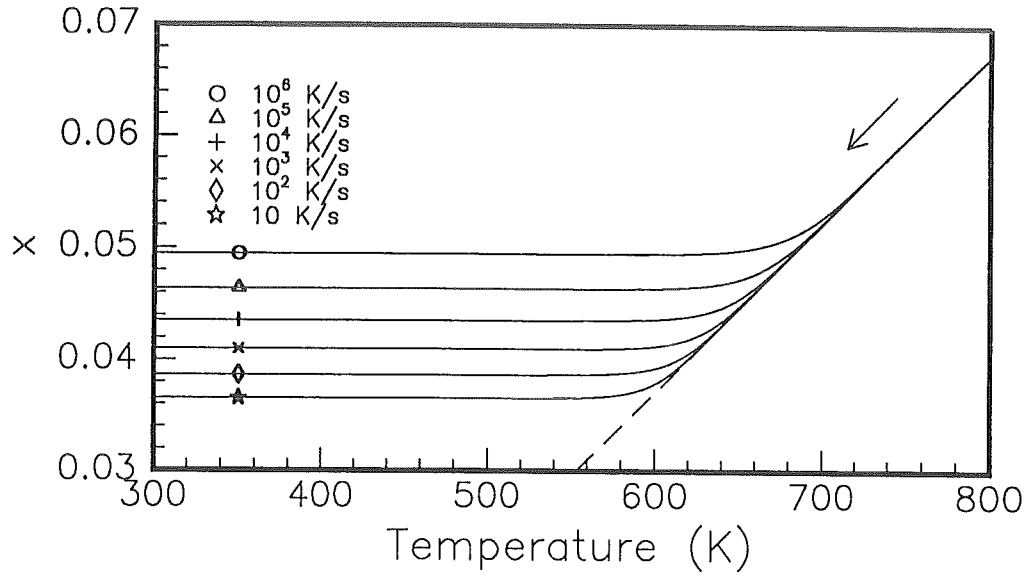

Figure 18: Calculated course of x during the quench from the liquid phase, at different quench rates.

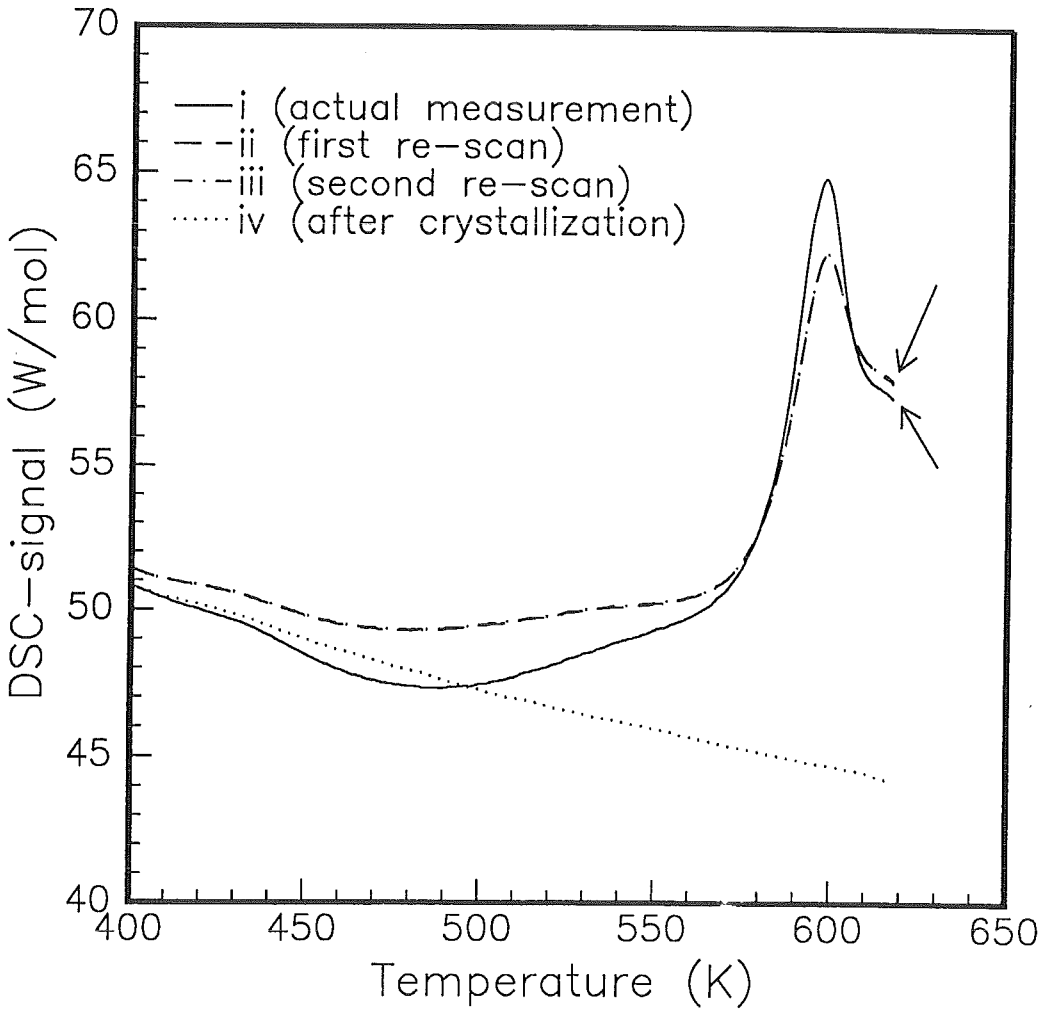

Figure 19: Irreproducibility of the level at the end of the first scan, as indicated by the arrows, possibly caused by variation of the temperature of the calorimeter at the beginning of the measurement.

4. Results

4.1 Introduction

The results of the measurements of the glass transition in amorphous $Pd_{40}Ni_{40}P_{20}$ are presented in this chapter.
The sample material was produced by the melt-spinning technique.
The basic principle of melt spinning is rapidly cooling a thin stream of liquid metal by spraying it onto a fast rotating water-cooled copper wheel. An illustration of this process is given in figure 17. The maximum obtainable quench rate is large, compared to other solidification methods: up to about 10^6 K/s.
The nucleation of the crystalline phase in undercooled $Pd_{40}Ni_{40}P_{20}$ is relatively slow, so that a quench rate below 10^6 K/s was sufficient to produce a completely amorphous metal. An indication of the cooling rate during the quench can be obtained by comparing the theoretical free volume after quenching at various rates with the free volume of the as-quenched material. The reduced free volume x_0 of the as-quenched material has been determined by speed-of-sound measurements [2] to be 0.041. Simulations at different cooling rates were made with the input parameters determined previously by other investigators [11], [2] from viscosity and speed-of-sound measurements. As can be seen from figure 18, the quench rate of our material is about 10^3 K/s according to these calculations. It must be kept in mind that this value is obtained on the assumptions that the cooling rate is constant, that the input parameters are valid at temperatures above the glass-transition temperature and that the value of 0.041 for the free volume of the as-quenched material is reliable. The other parameters, used in the free volume simulations, are: B=6600 K, T_0=355 K, E_f=160 kJ/mol and C_0=3.37 . 10^{25} s^{-1}.

4.1.1 Sample preparation

A problem that was encountered in the early stages of the experiments was irreproducibility of the measured level at temperatures higher than the transition peak (the metastable equilibrium level), between the first scan and the subsequent scans (see figure 19).
Apart from the variation of the temperature of the holder block which was dis-

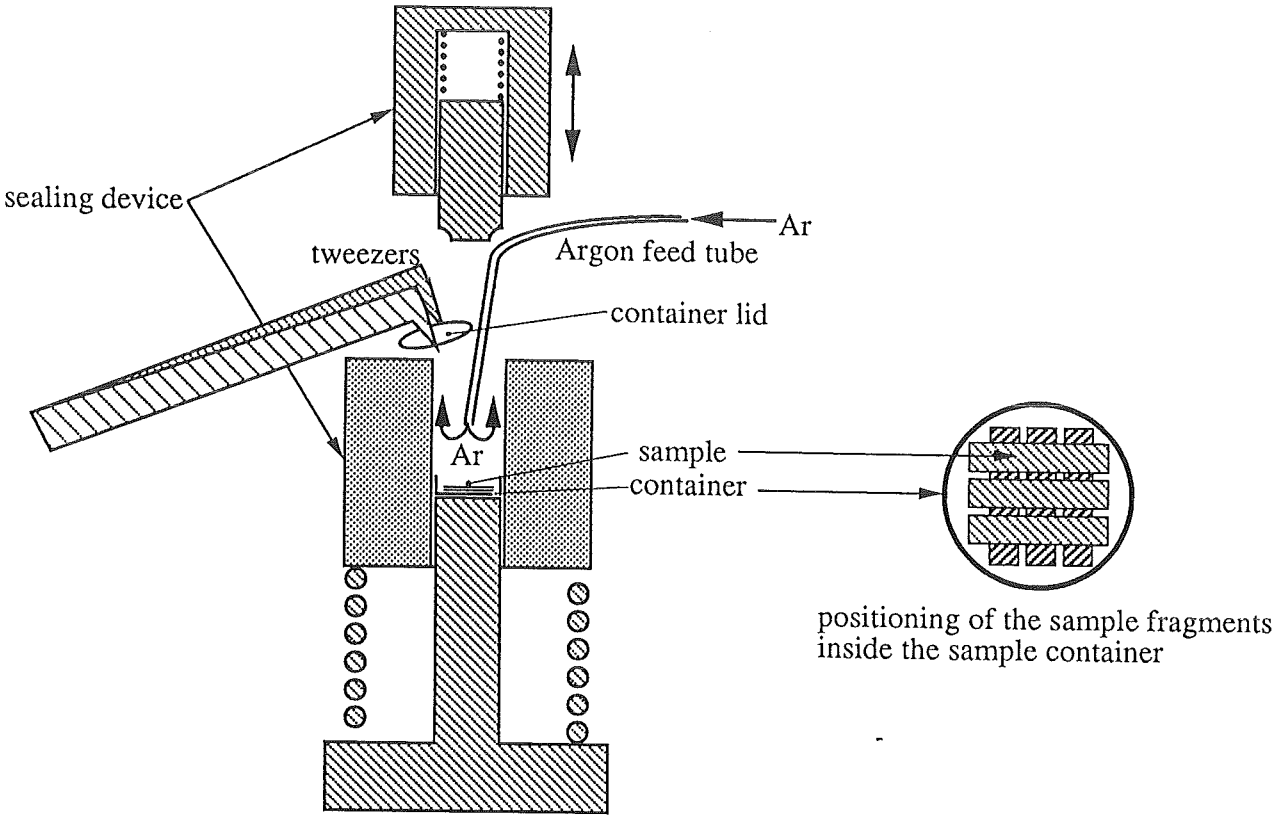

Figure 20: Schematic drawing of the way in which the sealing apparatus was fluxed with argon gas, to prevent oxygen inclusion in the sample container.

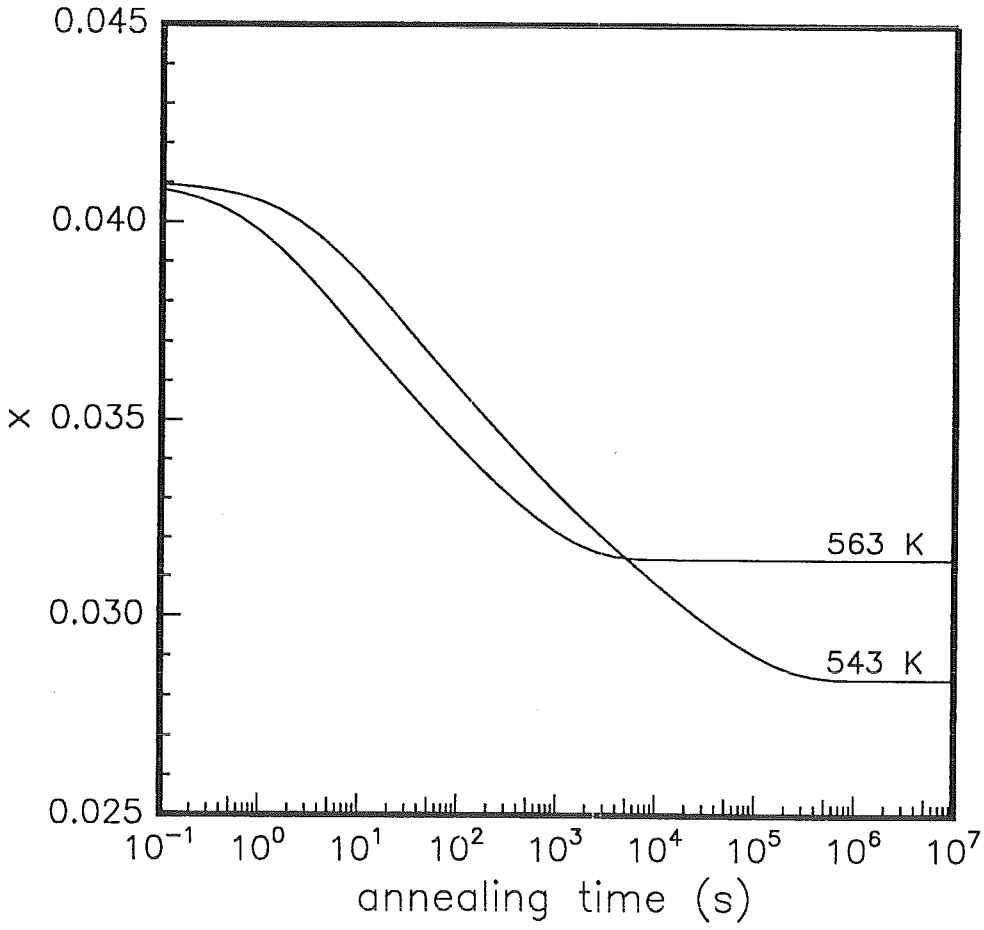

Figure 21: Calculated change of x during annealing of an as-quenched sample, at two different temperatures.

cussed in section 3.3.4, another possible cause for this phenomenon is oxygen from the air, trapped inside the sample container after the container is sealed. The oxygen would react with the aluminium of the container during the first scan, causing some additional exothermic signal which does not appear in later scans. To counter this effect, we tried to minimize the amount of oxygen present in the sample container by leading argon gas into the device by means of a small tube, just before sealing the container, as shown in figure 20. The combined effect of waiting for a half an hour before the measurement and sealing the sample container under argon gas provided an improvement of the reproducibility of the equilibrium level as can be seen by comparing figure 22 with figure 19.

4.2 Influence of pre-annealing on the glass-transition peak

Annealing an as-quenched sample causes its free volume to decrease. This way, samples with different free volume can be produced. The influence of the free volume at the start of the DSC-scans on the glass-transition peak is discussed here.

The samples can be divided into two groups, according to the applied annealing temperature. Two annealing temperatures were used, 543 K and 563 K.

The annealing treatment was performed in an open-ended tube furnace, with inert gas (helium) flowing through the tube to prevent oxidation of the samples.

The calculated free volume as a function of the annealing time at the two applied annealing temperatures is shown in figure 21. As can be seen in figure 21, the samples annealed at 563 K reach the 563 K equilibrium state after about 10,000 s. The samples annealed at 543 K reach the 543 K equilibrium after about 400,000 s. By annealing at 543 K, all possible values of x obtainable through annealing at 563 K can be reached. It is therefore interesting to verify whether two samples, annealed at different temperatures, but with the same value of x produce the same glass-transition peak in the DSC. If this is true, this is a strong indication that the free volume is the only parameter that determines the thermal behaviour in the glass-transition region. This will be shown to be true in section 4.2.2.

4.2.1 Four-scan method, internal reference

To ensure optimal reproducibility of the data, a special sequence of scans was

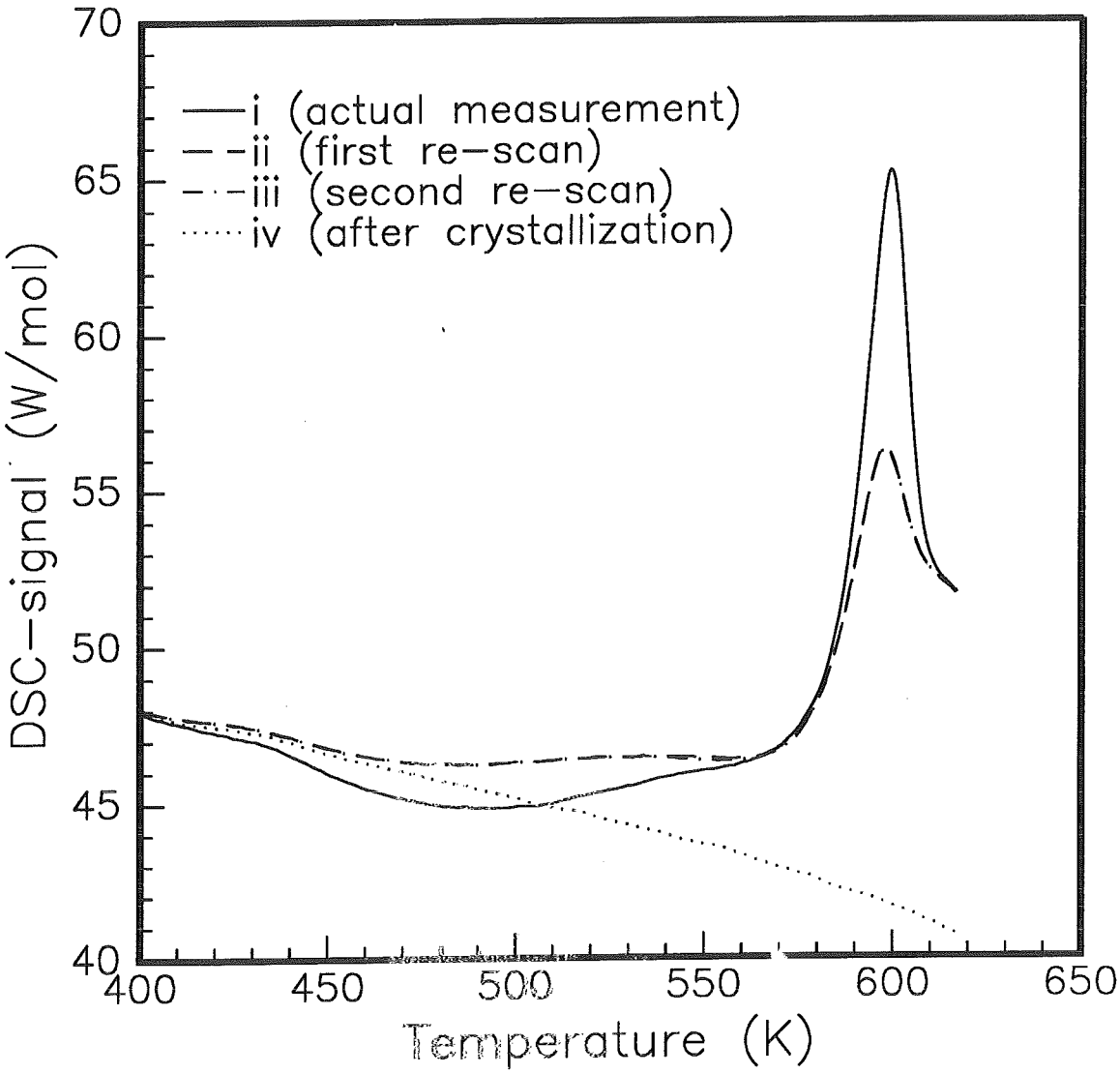

Figure 22: Example of an acceptable set of the four subsequent scans involved in each measurement.

adopted. Each sample was measured four times, without opening the calorimeter in between. Before each scan the temperature in the DSC was kept at room temperature for a half an hour. This was done to ensure a reproducible thermal state of the instrument before each scan.

The exceptionally high stability of the amorphous metal $Pd_{40}Ni_{40}P_{20}$ enables it to reach the metastable equilibrium state after the glass transition has been completed. This is a key fact in our measurement procedure.

Above the glass-transition temperature the free volume depends on the current temperature only. Therefore, by cooling the material from the temperature-dependent equilibrium state to room temperature at a defined cooling rate, the value of the free volume depends only on the selected cooling rate and not on any heat treatments before the equilibrium was reached. Reaching the equilibrium has, so to say, erased the thermal history of the sample.

Using the same cooling rate for each sample leads to a defined state at low temperature, which shall be called the reference state. Reheating in the DSC at a fixed heating rate results in a reproducible glass-transition peak. This peak provides an internal reference within the sample container. This has the advantage with respect to the usual calibration procedure that the value of the heat resistance between the sample and the rest of the instrument is the same for the measurement and the reference scan.

However, the internal calibration with the glass-transition peak, starting from the reference state, is not absolute, since the exact temperature of the glass transition is not known. Hence the usual calibration with pure metals can not be omitted. The additional calibration of the temperature axis is useful when observing the temperature difference between glass-transition peaks of different samples.

The measurement procedure consisted of four scans for each sample. An example of these four scans is shown in figure 22. In all four scans, the heating rates, as well as the cooling rates, were 40 K/min. All scans started at a temperature of 323 K and ended at 617 K, except for the crystallization scan, which ended at 713 K.

The first scan revealed the glass-transition peak as a function of the performed annealing treatment.

After the first scan, the sample was cooled to room temperature at a controlled rate to produce the reference state. After waiting for a half an hour, a second scan was taken, resulting in the reference glass-transition peak.

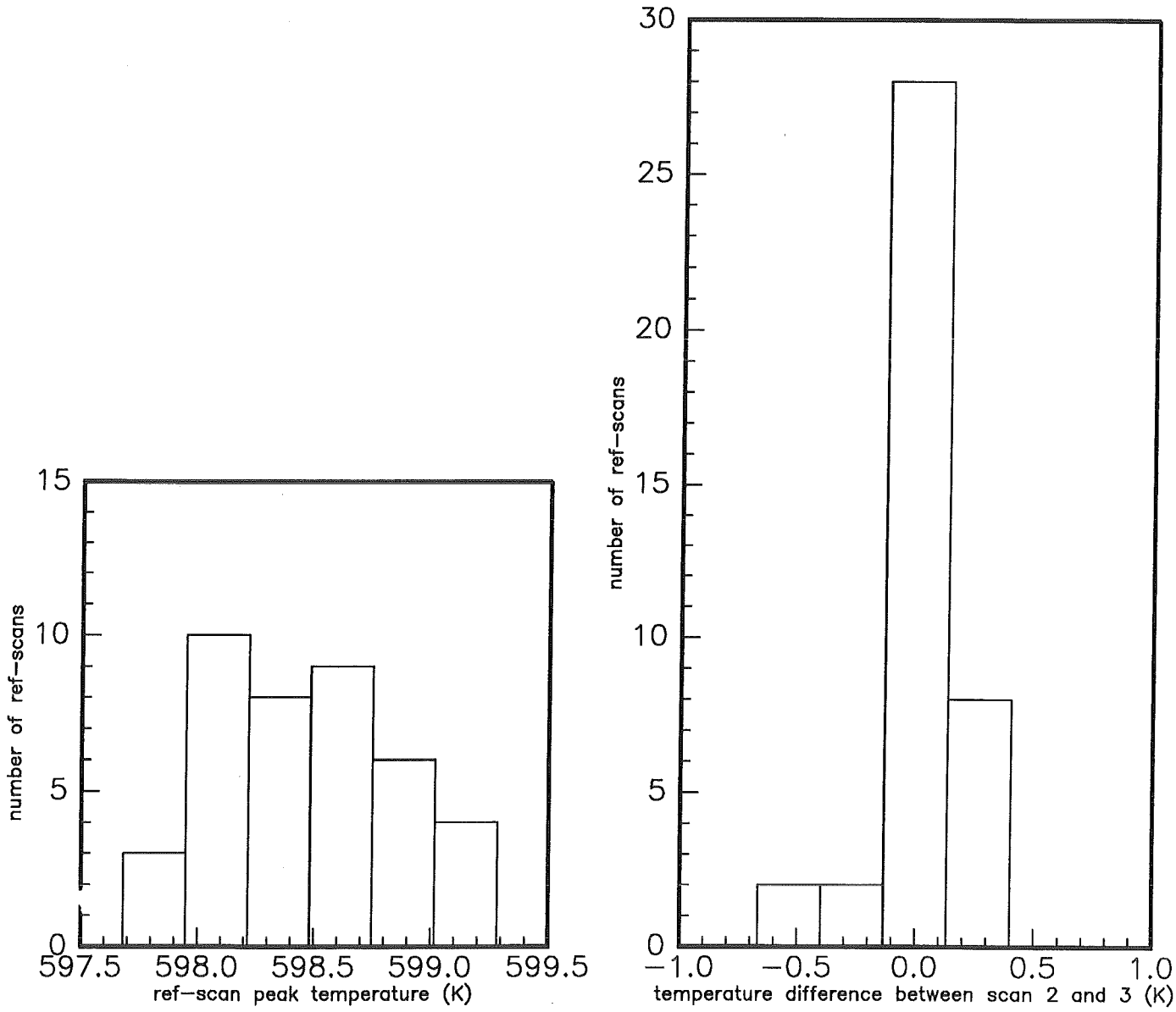

Figure 23: Distribution of the measured peak-temperature of the reference scans of all measurements, together with the distribution of the temperature difference between the two scans of each measurement

After the second scan, the procedure was repeated to produce another reference scan. The entire measurement was considered acceptable only if both reference scans had transition peak temperatures with a difference of 0.2 K, or less. The fact that most measurements were accepted is an indication of the good stability of the apparatus during the measuring period.

After the second reference scan, the material was heated to a temperature above the crystallization temperature. After cooling to room temperature and waiting for a half an hour, a scan of the crystallized sample was taken. The obtained data from this scan was taken as a reference differential power level, which was subtracted from the other scans. This was done with two objectives: firstly, to make the resulting scan independent of the baseline of the instrument and secondly to isolate the contribution of the structural relaxation to the specific heat from the normal specific heat of the sample, under the assumption that the normal specific heat is the same in the amorphous sample and in the crystalline sample and that it is the only contribution to the specific heat in the crystalline sample. All the experimental scans displayed in this work are the result of subtraction of the crystalline scan from the first scan (apart from the scans in figure 22).

In figure 22 it can be noted that the two reference scans appear as one, hence this is an acceptable measurement.

The distribution of the peak temperature of all reference scans and the distribution of the temperature difference between the two reference scans of each measurement are shown in figure 23. As can be observed, the width of the peak temperature distribution is larger than the width of the temperature difference distribution. These widths can be interpreted as a contribution to the inaccuracy of the measured glass-transition peak temperature, without respectively with the internal calibration procedure.

However, the scatter in the experimentally determined glass-transition peaks cannot be completely compensated by taking the reference-scan peak temperature of the measurement in question into account. A possible explanation for this fact is that during the first scan, the sample fragments, which have been forced into the aluminium container by sealing it, 'settle' by changing their shape and the shape of the container, causing the heat contact between the container and the sample chamber to change during the scan. This causes variation of the thermal lag of the sample during the scan which influences the measured data in a complex manner.

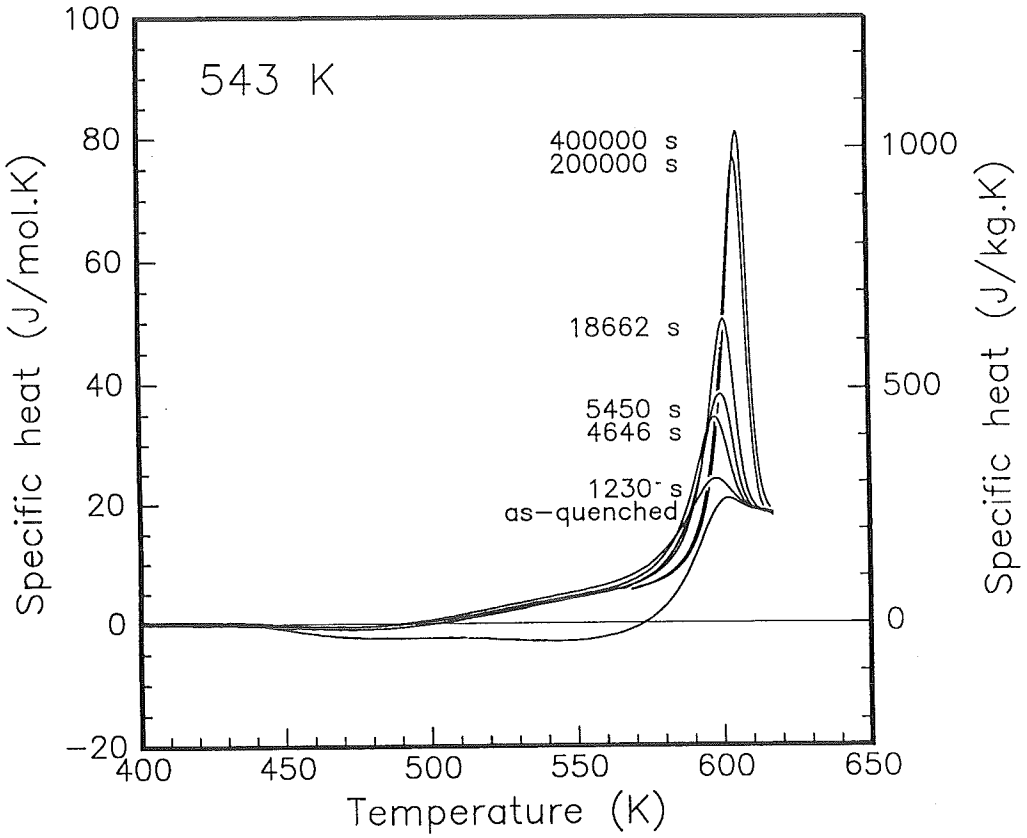

Figure 24: Experimental scans of the samples annealed at 543 K.

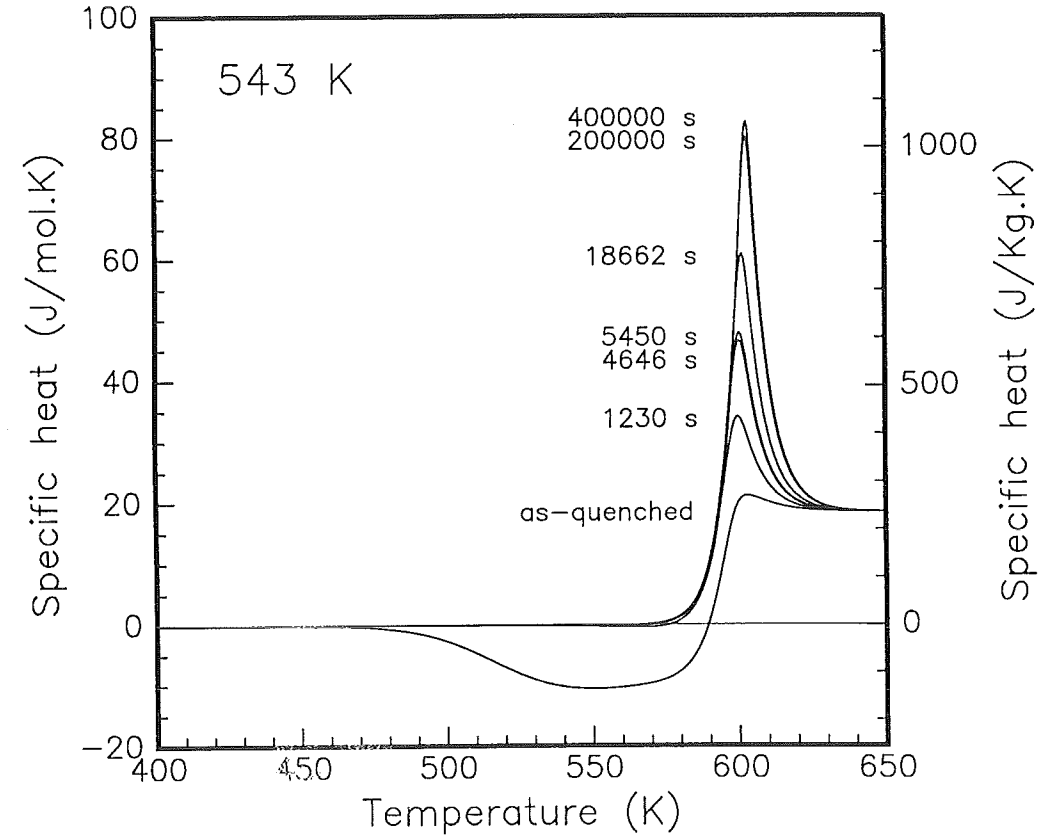

Figure 25: Calculated DSC-scans of $Pd_{40}Ni_{40}P_{20}$, annealed at 543 K.

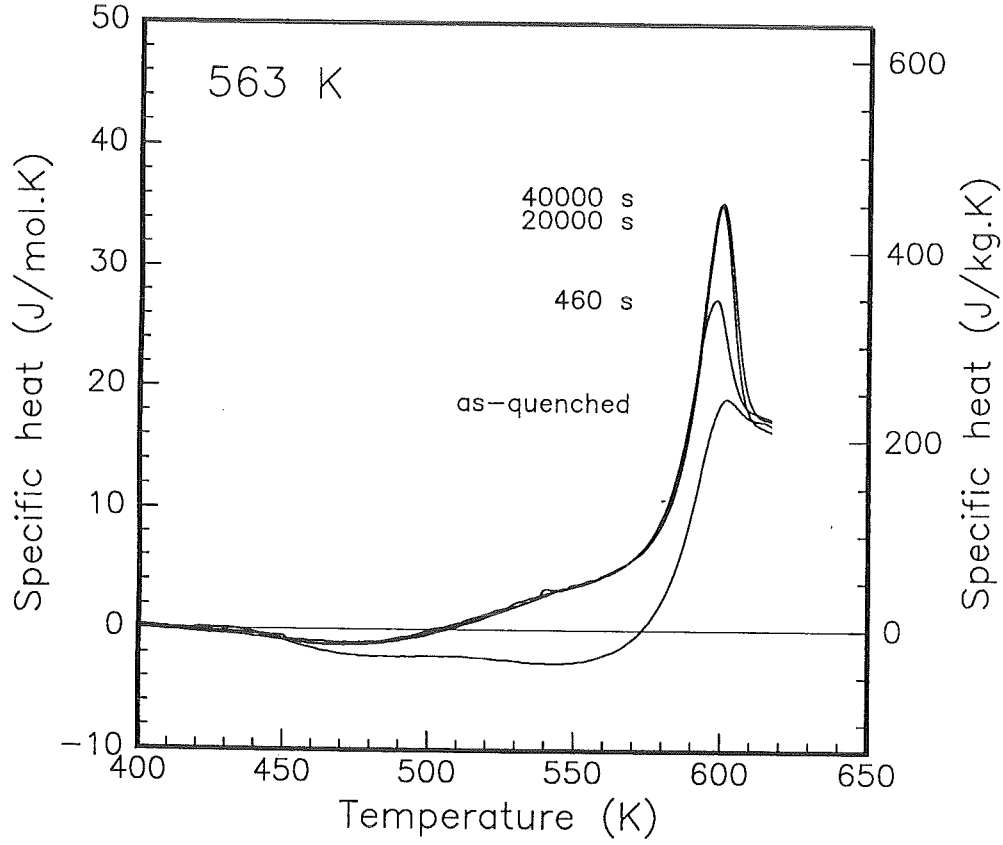

Figure 26: Experimental scans of the samples annealed at 563 K.

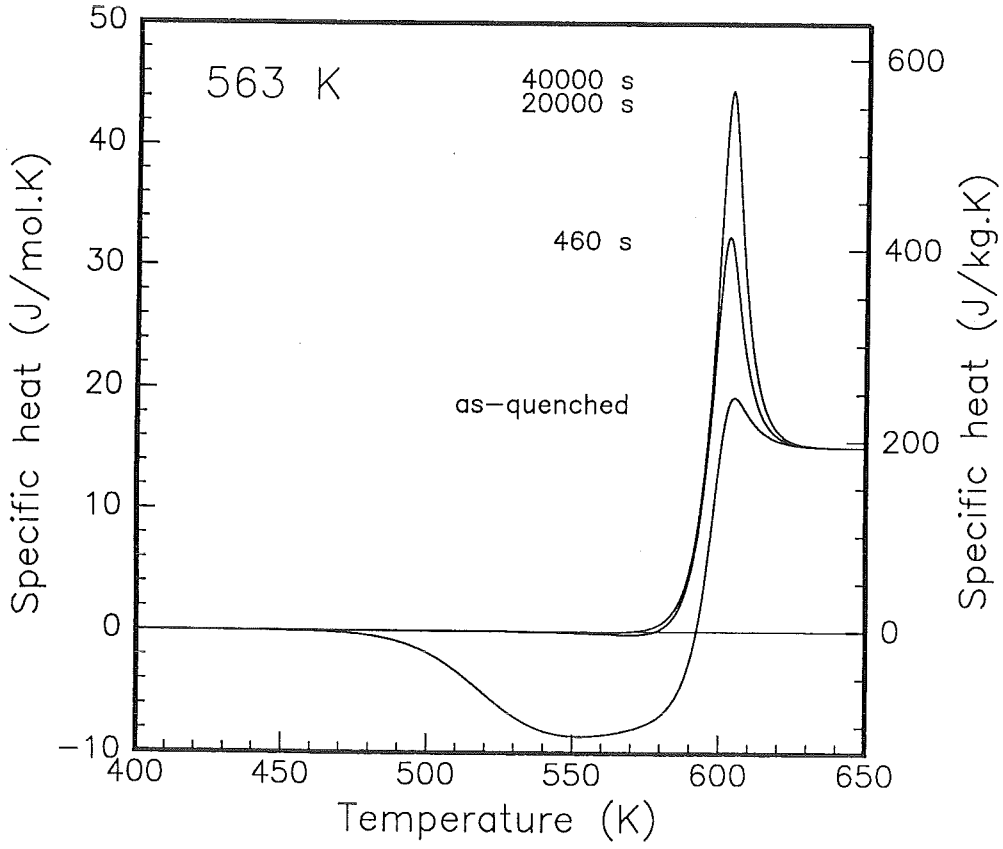

Figure 27: Calculated DSC-scans of $Pd_{40}Ni_{40}P_{20}$, annealed at 563 K.

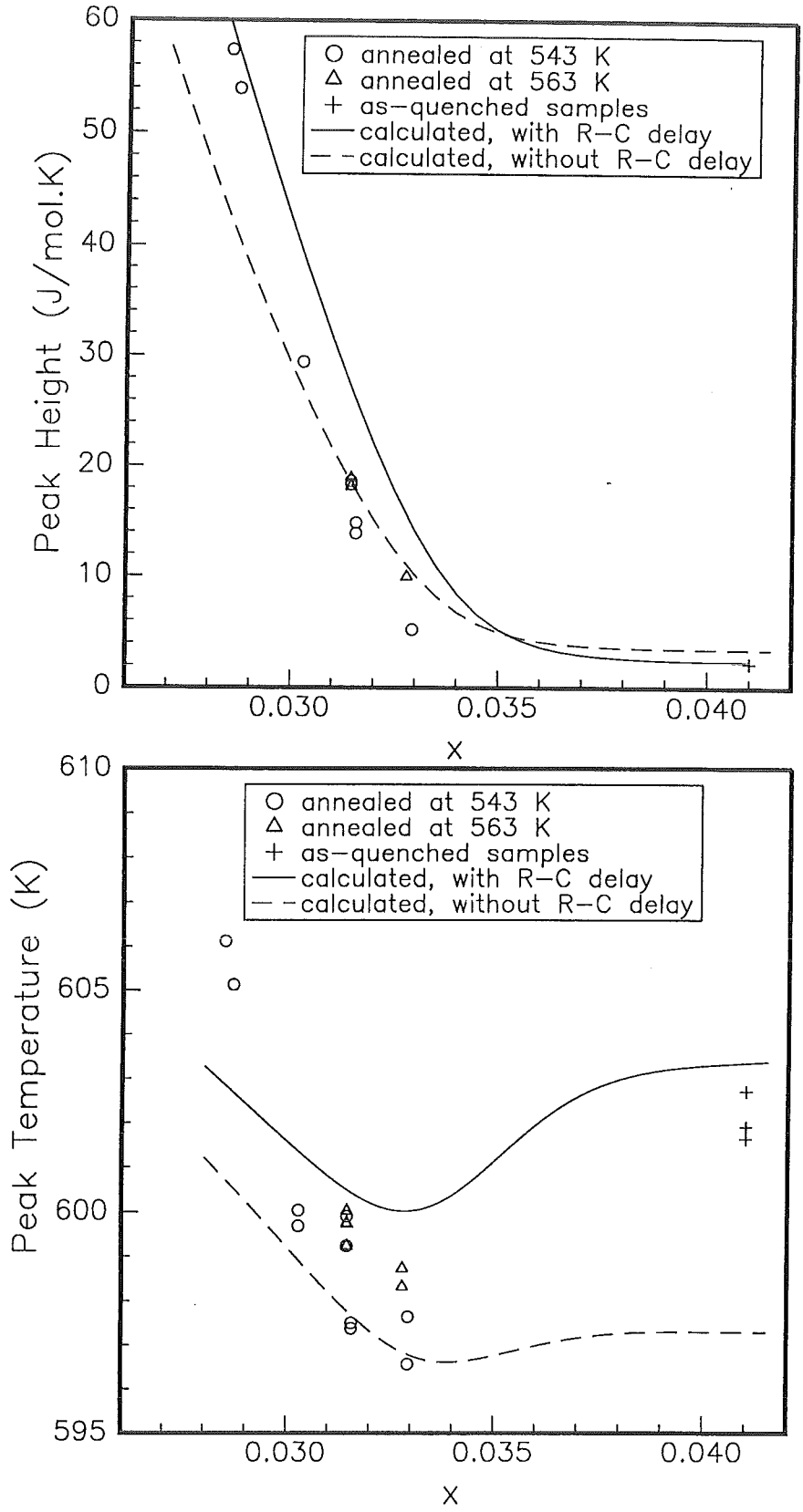

Figure 28: Measured peak temperature and the peak height, compared with the calculations.

Most measurements had peak temperatures for both reference scans with a difference of 0.2 K or less and were therefore accepted measurements.

4.2.2 Results of the glass-transition peak as a function of the annealing treatment

The central issue of this work was to investigate the influence of pre-annealing treatments on the shape and the position of the glass-transition peak. This investigation can show to which extent the free volume theory is able to describe the glass transition of the material $Pd_{40}Ni_{40}P_{20}$.
Prior to a measurement, the as-quenched material was annealed either at 543 K or at 563 K. A range of annealing times was applied, up to 40,000 s at 563 K and up to 400,000 s at 543 K. This produced material with a range of different values of initial free volume x (see figure 21). The glass-transition peak was observed in a DSC experiment, as described in the previous section.
The objective of these measurements was to investigate the dependence of the observed glass-transition peak on the calculated initial free volume x_0. This dependence was subsequently compared with the dependence of calculated DSC-scans on x_0, using the free volume theory.
The experimental glass-transition peaks are shown in figure 24 and 26. The calculated scans, with the thermal lag of the DSC taken into account, are shown in figure 25 and 27.
As can be seen, the height of the experimental peaks increases with increasing annealing time. The peak temperature initially decreases with increasing annealing time, but at longer annealing times, the peak temperature shifts back. These features are also found in the calculated curves. Because the free volume is a monotonously decreasing function of the annealing time, this behaviour of the peak temperature can also be observed by plotting it as a function of the free volume. This has been done in figure 28, where the height of the peak, measured from the equilibrium (end) to the level of the maximum, and the temperature of the maximum are plotted as a function of the free volume after the annealing treatment.
In the same plot, the calculated position of the peak is shown as a function of x. The shift in the peak temperature is comparable to the shift in the calculated scans. Calculations in which the thermal lag in the DSC is not taken into account

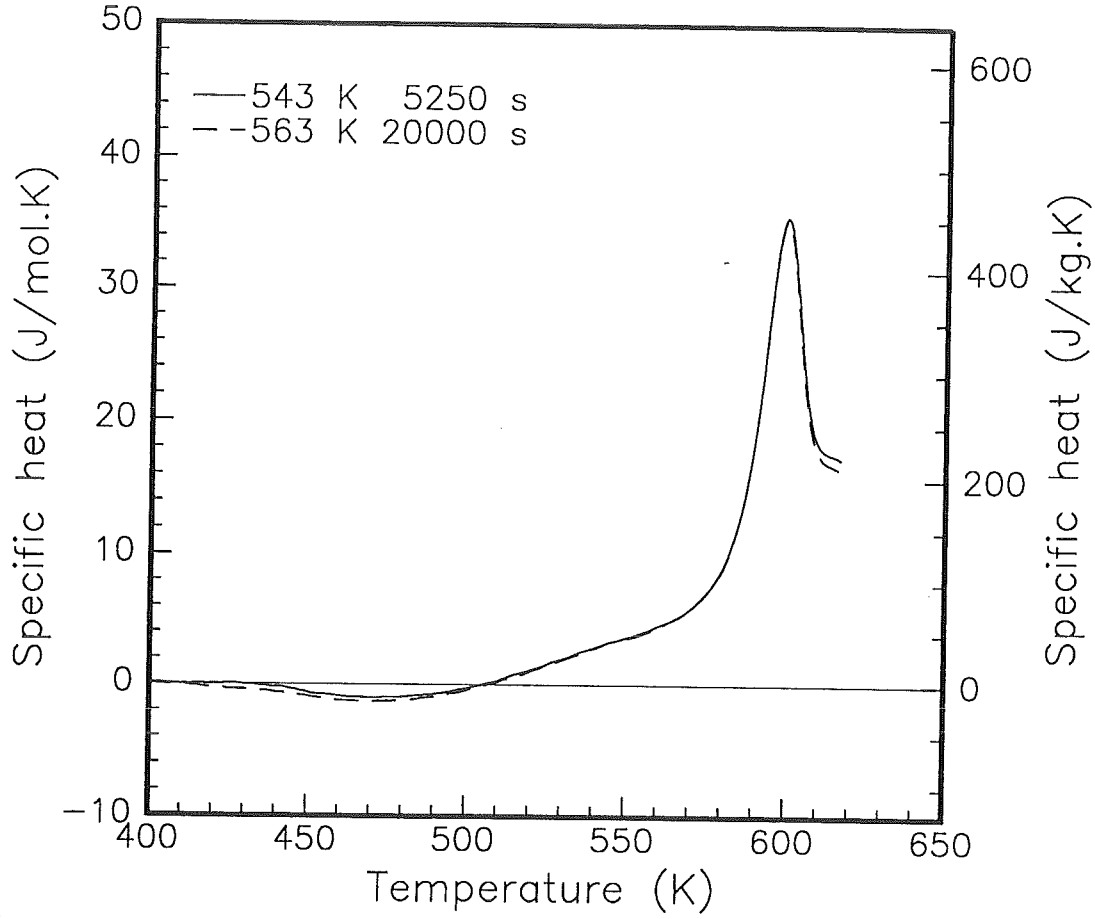

Figure 29: Two scans, with different annealing temperatures, but with the same calculated value x_0 of x at the beginning of the scan ($x_0 = 0.03145$).

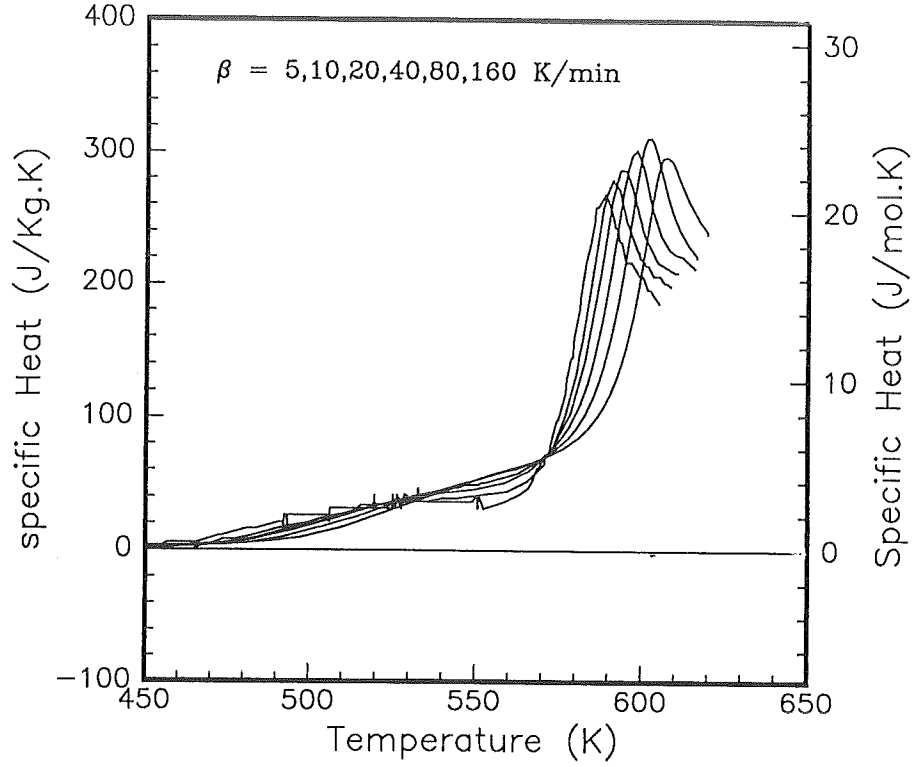

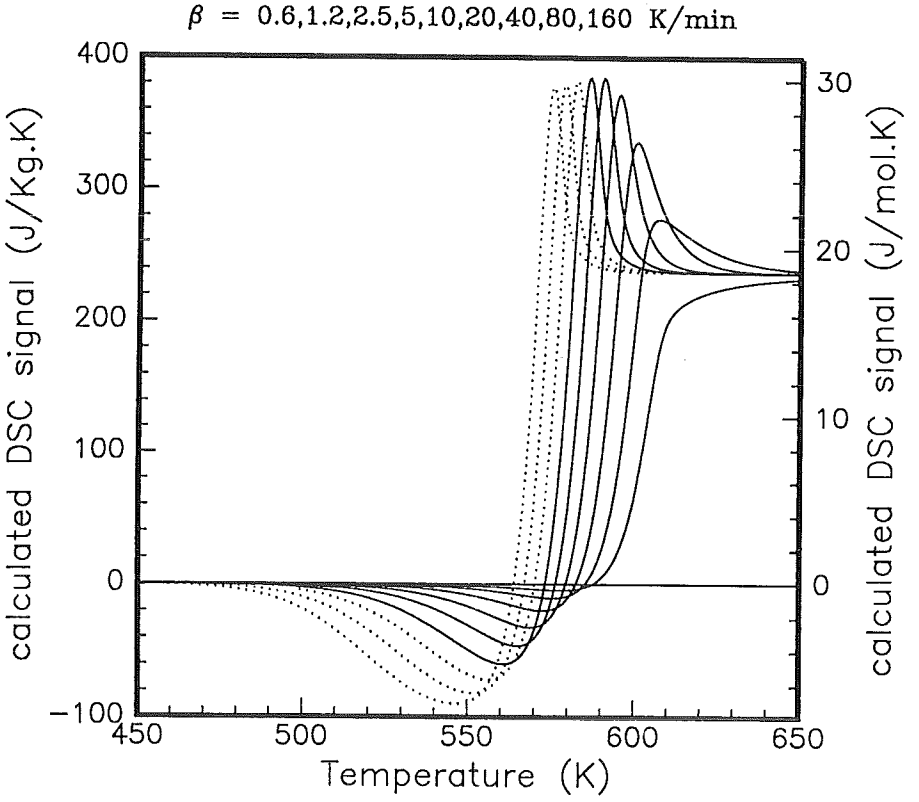

Figure 30: Measured and calculated scans at heating rates between 5 and 160 K/min (solid lines). Dotted lines $\beta = 0.6$ - 2.5 K/min.

result in a smaller shift in temperature and hence in worse agreement with the measurements. Taking CSRO into account could lead to further improvement of the agreement between the measured and the calculated data. At present, effort is being taken to implement CSRO into the calculations of the DSC signal.
A test whether x is the only material parameter that determines the glass-transition behaviour of the material is performed by comparing the shape of the transition peaks of material annealed at two different temperatures and annealing times, but with the same resulting value of x, *viz.* $x = 0.03145$. The result of this test is shown in figure 29. The peaks are of the same shape and position, since they appear as one curve. This means that the material follows the same subsequent states in the path to equilibrium up to the equilibrium situation of the highest annealing temperature.

4.3 Influence of the variation of the heating rate on the glass-transition peak.

4.3.1 Experimental results on the variation of the heating rate.

The observed glass-transition peak of a material with a certain value of x at the beginning of the scan depends on the chosen heating rate. A higher heating rate results in a higher peak temperature. This can be observed in figure 30, where measurements of the glass transition at different heating rates are presented. All these measurements were performed on the same sample. A reproducible value of x at the beginning of each scan was attained in the same way as with the reference scans in the four-scan method: after reaching equilibrium at the end of each scan, the sample was cooled down at a controlled rate of 40 K/min. This produces an initial value of x of 0.0343 for the next scan. In the same figure, the calculated scans at those varying heating rates are presented. The height of the peak of the measurements increases up to 80 K/min, but the height of the 160 K/min scan is lower than the scan at 80 K/min. The calculated scans show the same tendency, although the decrease of the peak height starts at lower heating rates. This characteristic is not shared by calculations with no thermal lag, where the peak height increases continuously for higher heating rates. This fact favours the thermal-lag approach, as described in chapter 3. The fact that the obtained values for R, C and α, as given in the sections 3.3.3 and 3.4, cannot describe the

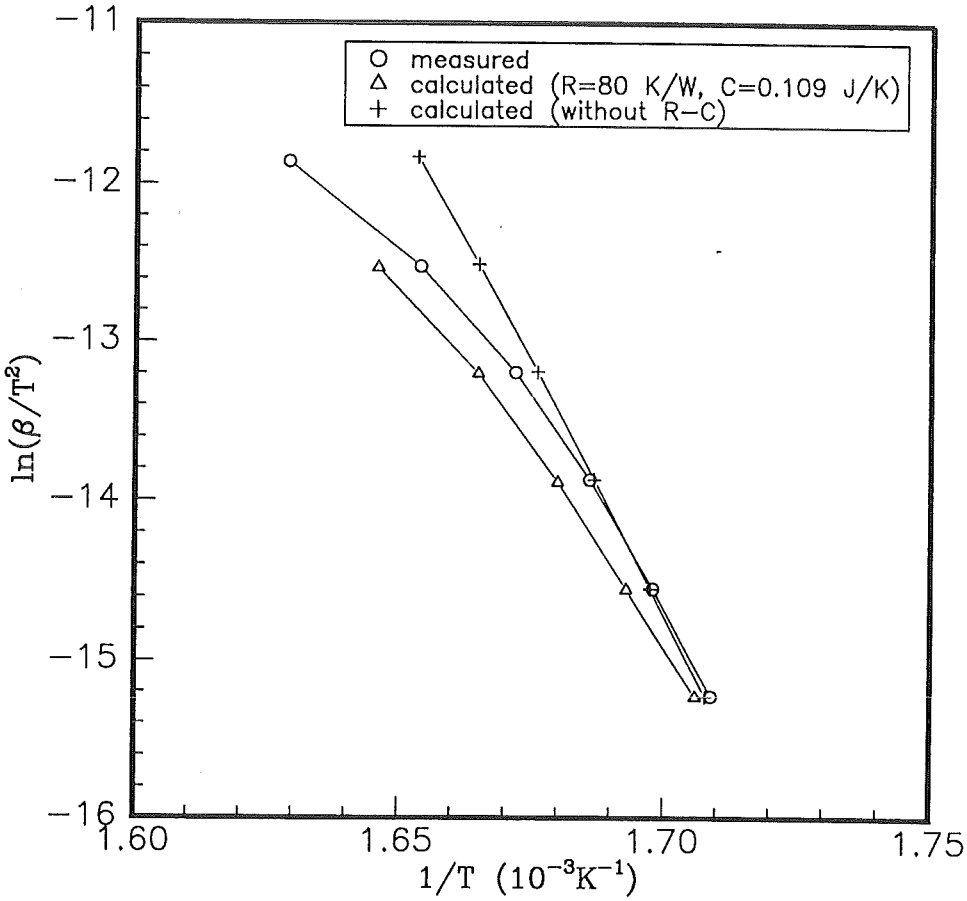

Figure 31: Kissinger plot of measured and calculated data, in the heating-rate range between 5 and 160 K/min. Calculated data both with and without thermal lag.

scans completely (*e.g.* in the calculated scan at 160 K/min the transition peak has vanished), is presumably caused by the fact that the R-C model is too simple to characterize the thermal lag in the DSC completely.

4.3.2 Applicability of the so-called Kissinger plot to the glass transition

In experiments in which the sample is heated at a constant rate, the activation energy of a thermally activated process can usually be determined by making a so-called Kissinger plot of the process. The construction of the Kissinger plot involves measuring the peak temperature of the process at various heating rates. The dependence of the peak position on the heating rate is plotted in a special way, usually resulting in a straight line, from which the activation energy can be determined. The Kissinger analysis is based on the assumption that the process in question has a Boltzmann temperature dependence and first-order kinetics:

$$\frac{dc_x(t)}{dt} = -c_x(t)\nu_0 \exp\left(\frac{-E_a}{R\beta t}\right), \tag{19}$$

where c_x is the fraction left of the component to transform, ν_0 is the attempt frequency, E_a is the activation energy of the process and β is the chosen heating rate.

The maximum transition rate is achieved when the second derivative of $c_x(t)$ is zero. Elementary mathematics leads to the equation behind the Kissinger plot, *viz.*:

$$\ln\left(\frac{\beta}{T_{max}^2}\right) = \frac{-E_a}{R} \cdot \frac{1}{T_{max}} - \ln\left(\frac{E_a}{\nu_0 R}\right). \tag{20}$$

Here, T_{max} is the temperature of the maximum transition rate. Plotting $\ln(\beta T_{max}^{-2})$ versus T_{max}^{-1} gives a straight line with a slope $\frac{-E_a}{R}$ and an intersection with the ordinate at $\ln\left(\frac{E_a}{\nu_0 R}\right)$, if the observed process is indeed subject to the conditions stated at the beginning.

The Kissinger analysis is sometimes applied to the glass transition *e.g.* in ref. [12]. Measurements and simulations of the glass-transition peak show a more or less linear dependence in the Kissinger plot (figure 31). This could lead to the conclusion that the parameters of the relaxation process can be derived from the Kissinger plot. The values for E_a and ν_0 that were derived from figure 31 are displayed in table 1.

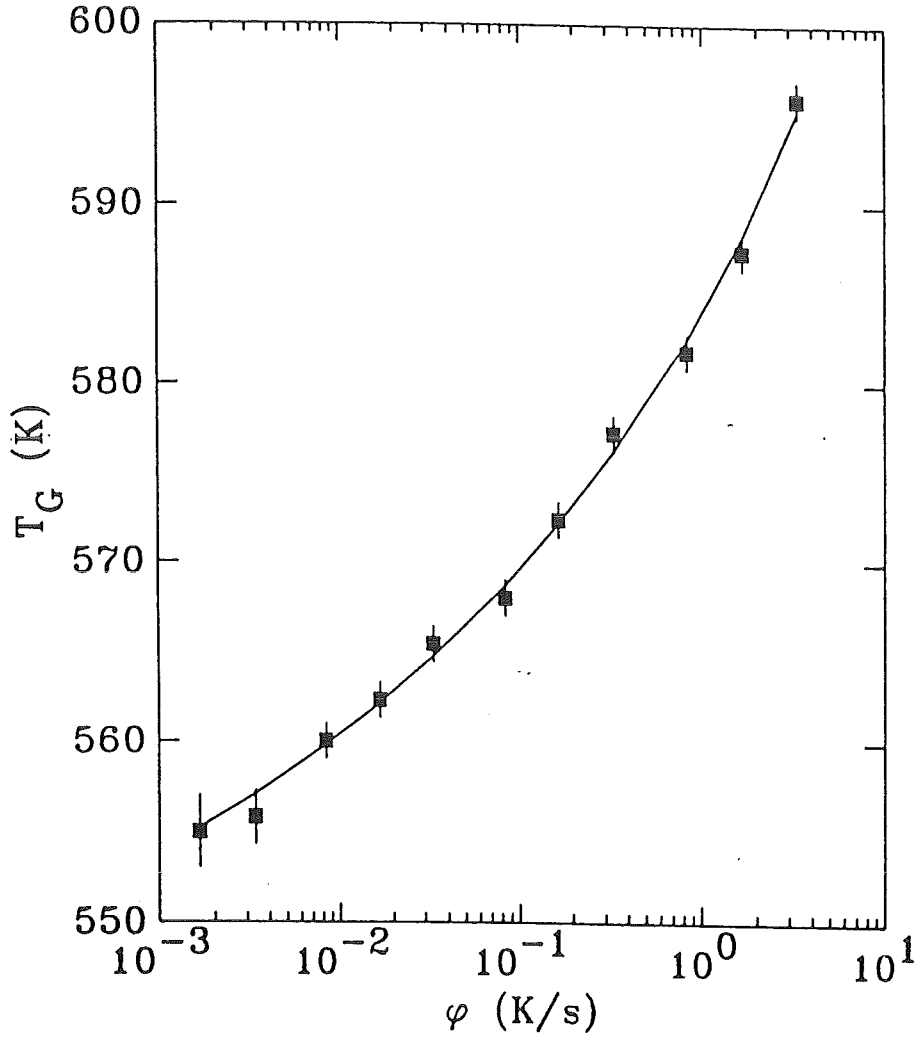

Figure 32: Onset temperature of the glass-transition peak of amorphous $Pd_{40}Ni_{40}P_{19}Si_1$, measured at low heating rates φ by Brüning [13].

Table 1: Values of the activation energy E_a and the attempt frequency ν_0 as derived from the Kissinger plot (figure 31) for the experimental scans and the calculated scans.

data source	E_a (kJ/mol)	ν_0 (s^{-1})
Measured	350	$2.2 \cdot 10^{29}$
Calculated, with R-C	377	$4.5 \cdot 10^{31}$
Calculated, without R-C	520	$3.9 \cdot 10^{44}$

The derived values for ν_0 are unphysically high. This can be explained by the fact that the structural ordering of metallic glasses, with its temperature-dependent equilibrium state (and therefore time-dependent in a non-isothermal treatment), does not fulfill the requirements stated above.

The fact that the Kissinger analysis is not justified for the glass transition, is demonstrated in the case of the calculated scans without thermal lag by the difference between the obtained value of the activation energy from the Kissinger plot and the input value of the activation energy in the calculation. The value for E_a, obtained from the Kissinger plot is 520 kJ/mol, whereas the input value of the activation energy E_f in the simulations is only 160 kJ/mol. This observation calls for caution when basing quantitative conclusions on the Kissinger plot of the glass transition. It can also be seen that the occurrence of thermal lag strongly influences the outcome for E_a.

4.4 The glass transition at very low heating rates

Although the idea that the glass transition is a kinetic phenomenon that depends on the chosen heating rate and the thermal history of the sample, is well established, sometimes claims are made that under special circumstances, the glass transition becomes a material constant. Here, a claim by Brüning [13] that the glass transition becomes a sharp, fixed transition at very low heating rates ($< 10^{-5}$ K/s), is investigated.

Brüning presented a set of measurements of glass-transition peaks of the amorphous metal $Pd_{40}Ni_{40}P_{19}Si_1$, measured at heating rates down to $1.7\ 10^{-3}$ K/s (= 0.1 K/min).

The experimental data from Brüning is presented in figure 32. Brüning used a

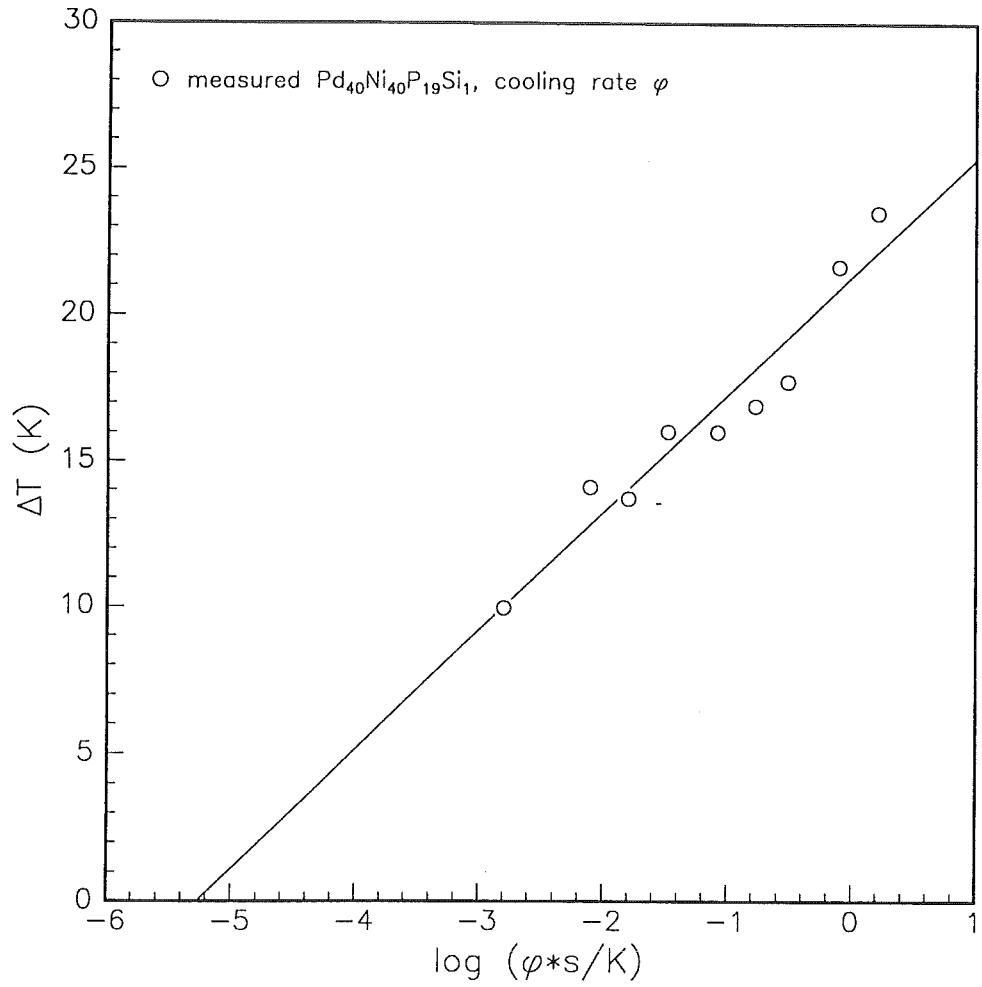

Figure 33: Width of the transition peak of $Pd_{40}Ni_{40}P_{19}Si_1$ as a function of the heating rate, from ref.[13].

special sequence of scans for his measurements. The as-quenched material was brought to a temperature above the glass-transition range so that it was in the equilibrium state. From the equilibrium, the sample was cooled down at the same (low) rate as it would be heated up in the subsequent measurement. Brüning claims that the advantage of this procedure is that the complete measurement is performed on a single time scale. A possible advantage of this method is the fact that the difference between the value of x at the beginning of the scan and x when the equilibrium is reached, is more or less independent of the heating rate, resulting in a similar shape of the scan for each measurement. In the method used by us, we cooled down at the same rate from the equilibrium before each measurement, producing a reproducible initial state before the scan. The advantage of our method is that the initial condition is the same for each scan, so the results are not influenced by errors in the cooling-rate dependence of x.

Brüning used a Vogel-Fulcher type function to fit the heating-rate dependence of the onset temperature:

$$T_G = T_G^0 + \frac{A}{\ln\left(\frac{B}{\beta}\right)}, \tag{21}$$

where T_G is the observed onset temperature of the glass-transition peak, T_G^0 is the lower limit to which the experimental onset temperature allegedly would converge in the case of infinitely slow cooling and heating, A and B are fit parameters and β is the heating rate. The fit parameters, including T_G^0, can be found by varying the heating rate β. The line connecting the experimental data in figure 32 is the best fit, according to Brüning. The value of T_G^0, determined with this fit is (518 $\pm$ 6)K, A=(538 $\pm$ 100)K and B=(3700 $\pm$ 2000)K/s.

A problem with this analysis is that a lower limit for the glass transition is assumed a priori. The fact that a certain value of T_G^0 results from fitting experimental data points with this function does not imply that there really is a lower value for the glass transition temperature.

A second evidence for a fixed glass transition according to Brüning, is the fact that the width ΔT of the transition peak is proportional to the logarithm of the heating rate. At some very low heating rate, the peak width would become zero, corresponding to a 'sharp' transition. The width is determined in this case by the difference between the onset temperature of the peak and the temperature at the maximum. The data Brüning presented is shown in figure 33, where the measured peak width is plotted as a function of the logarithm of the heating rate.

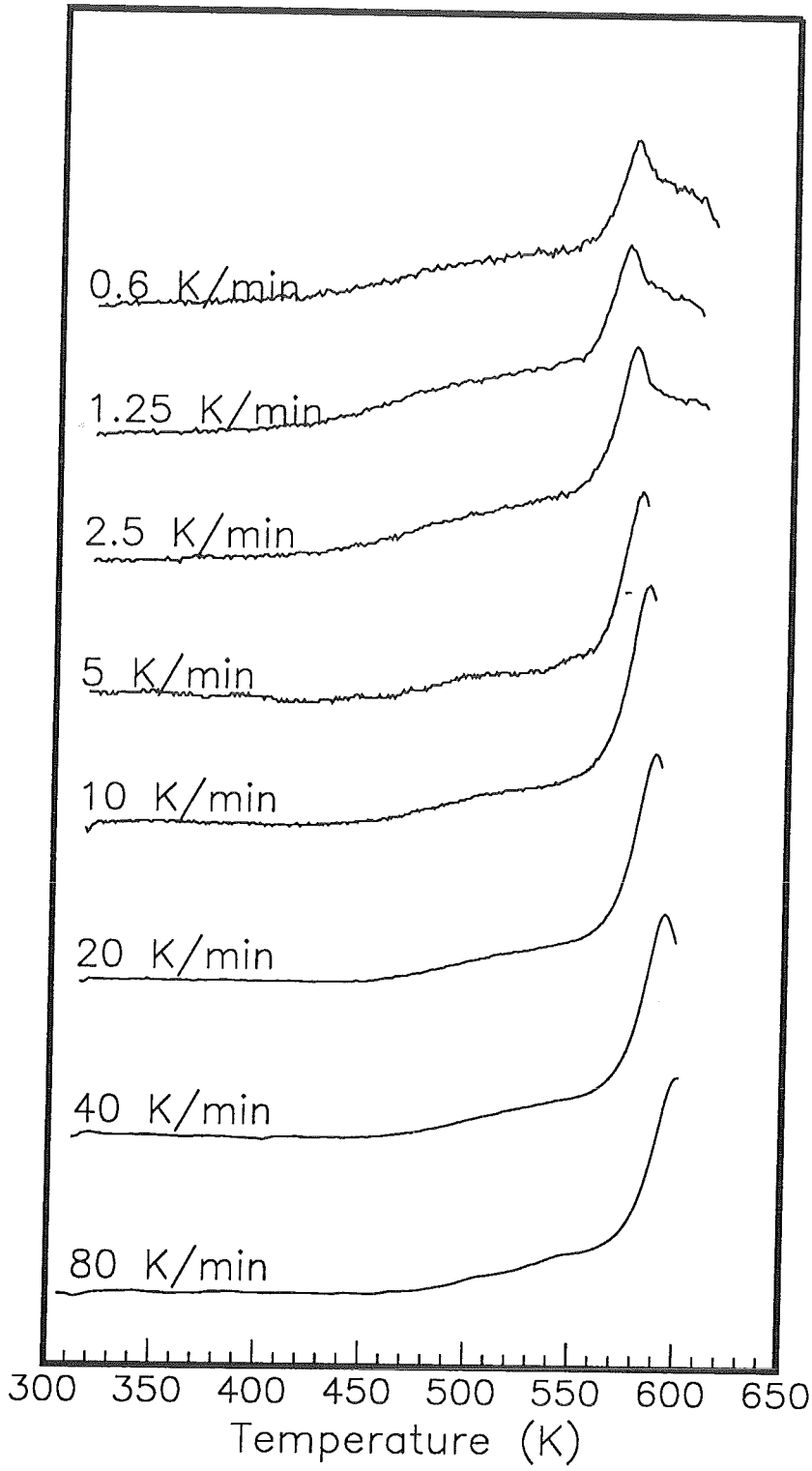

Figure 34: Scans of $Pd_{40}Ni_{40}P_{20}$, at various heating rates

The extrapolated line through the data points intersects with the ordinate at a heating rate of about 10^{-5} K/s, where the glass transition might become a 'sharp' transition, according to Brüning.

We were interested whether $Pd_{40}Ni_{40}P_{20}$ shows the same characteristics at low heating rates. Measurements were performed at heating rates down to 0.01 K/s with $Pd_{40}Ni_{40}P_{20}$, both using a heating-rate dependent state before the measurement the way Brüning proposed and using a reference state before the measurement by cooling at a fixed rate of 40 K/min from equilibrium. The scans that were produced this way are shown in figure 34. The scans at low heating rates are observably decorated with experimental noise which is caused by the fact that the differential power signal becomes small at low heating rates. This fact was compensated partly by using large samples at low heating rates ($\approx$ 70 mg), about as much as would fit into a sample container.

The peak width is plotted in figure 35 as a function of the logarithm of the heating rate the same way Brüning did, together with the data on $Pd_{40}Ni_{40}P_{19}Si_1$, measured by Brüning.

The peak width need not become zero at low heating rates, as Brüning claimed. This can be observed when the width of the peak on a time scale (the peak width on the temperature scale divided by the scanning rate) is plotted as a function of the heating rate, instead of the width on the temperature scale (see figure 36). The width of the transition peak on a time scale keeps increasing as the heating rate decreases. This can be understood because the differential power signal becomes very low, the duration of the transition must increase proportionally to result in the same total transition heat. Therefore, the width of a transition peak *cannot* become zero in a scanning experiment as DSC.

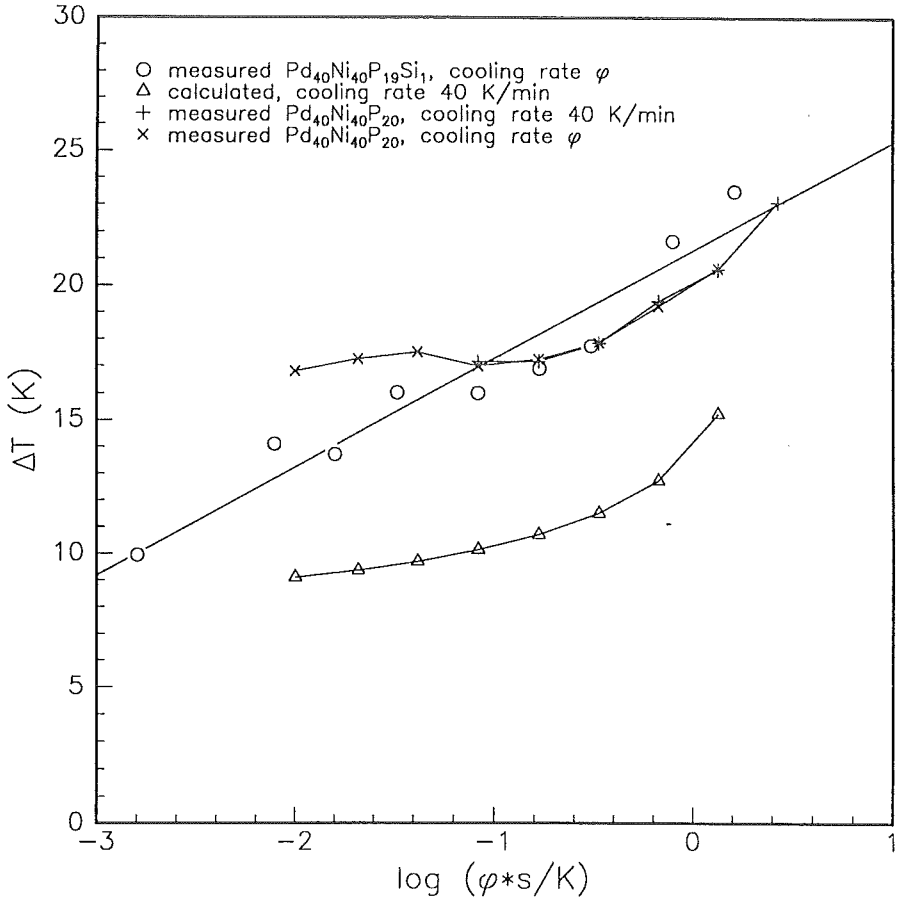

Figure 35: Width of the measured scan on the temperature scale as a function of the heating rate.

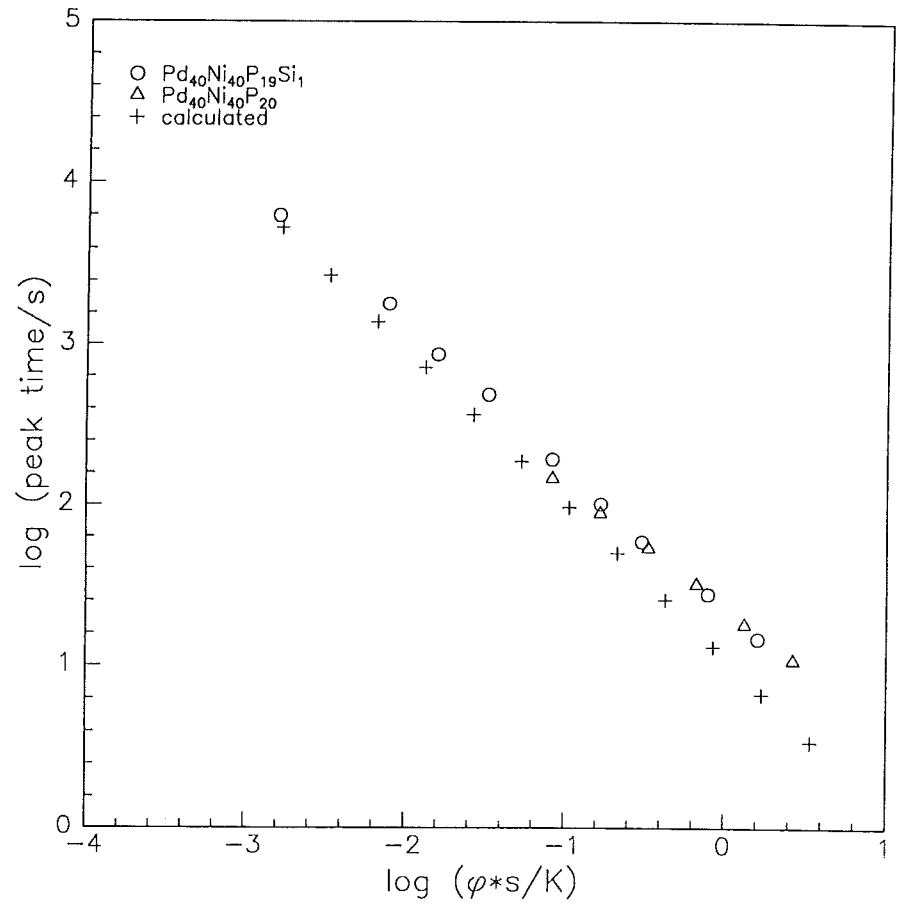

Figure 36: Duration of the glass-transition peak as a function of the heating rate, for measured and calculated scans.

5. Conclusions

The influence of pre-annealing on the glass-transition peak of the amorphous metal $Pd_{40}Ni_{40}P_{20}$ was investigated, using a Perkin-Elmer DSC-7 differential scanning calorimeter.

It was found that the Free Volume Theory, taking only free-volume changes into account, describes the measured glass-transition peaks well. Especially the test with two samples, annealed at different temperatures, but with the same value of the free volume at the start of the experiment, showed that the glass transition of amorphous $Pd_{40}Ni_{40}P_{20}$ can be described by the use of a single parameter.

The shape of the glass-transition peak is not completely in accordance with the experimentally determined glass-transition peak. In addition, the heating-rate dependence of the maximum of the transition temperature differs between the experimental scans and the theoretical scans. Using a simple R-C model to take the thermal lag of the calorimeter into account improves both the agreement of the peak width and the agreement for the heating-rate dependence of the maximum of the peak considerably. However, the shape of the experimental scans is not reproduced completely by the calculated scans. A possible explanation of this fact is that the value of the thermal resistance R varies during the measurement, due to change of the shape of the sample during the measurement.

The four-scan method, which provides an internal reference for each measurement, has proved unable to compensate for all experimental scatter. This problem is also believed to be caused by change of the heat resistance inside the sample container due to change of the shape of the sample fragments during the scan.

It is therefore concluded that an improvement of the thermal contact between the calorimeter and the sample would improve the reproducibility of the measured glass-transition peaks considerably.

Tests were performed to determine whether the glass transition becomes a material constant at very low heating rates, as claimed by R. Brüning [13].

No real evidence was found to deny these claims, but our measurements, together with free-volume simulations, indicate that although the width of the peak on the temperature scale keeps decreasing, it becomes wider on the time scale. This is caused by the fact that the glass transition has a finite transition heat.

References

[1] A. van den Beukel and S. Radelaar, Acta metall. **31** (1983), 419-427.

[2] G.W. Koebrugge, On the kinetics of structural relaxation in some metallic glasses, Ph.D. Thesis, T.U. Delft (1991).

[3] M.H. Cohen and D. Turnbull, J. Chem. Phys. **31** (1959), 1164-1169.

[4] M.H. Cohen and G.S. Grest, Phys. Rev. B **20** (1979), 1077-1098.

[5] S.S. Tsao and F. Spaepen, Acta metall. **33** (1985), 891-895.

[6] A. van den Beukel and J. Sietsma, Acta metall. mater. **38** (1990), 383-389.

[7] G.W.H. Höhne and E. Glöggler, Thermochimica Acta **151** (1989), 295-304.

[8] J.H. Flynn, Status of Thermal Analysis, O. Menis, Ed., NBS Special Publ. **338** (1970), 119-136.

[9] J.H. Flynn, Analytical Calorimetry **3**, R.S. Porter and J.F. Johnson, Eds., Plenum Press, New York (1974), 17-44.

[10] R.F. Speyer and S.H. Risbud, Thermochimica Acta **131** (1988), 211-240.

[11] P.A. Duine, J. Sietsma and A. van den Beukel, Acta metall. mater. **40** (1992), 743-751.

[12] R. Brüning, Structural relaxation and the glass transition in metallic glasses, Ph.D. Thesis, McGill University, Montreal, Canada (1990).

[13] R. Brüning and K. Samwer, The glass transition on long time scales, preprint of publication in Phys. Rev. B.